TECHNISCHE UNIVERSITÄT WIEN
Vienna University of Technology

INSTITUT FÜR PHOTONIK
Photonics Institute

DIPLOMARBEIT

der Technischen Universität Wien

NUMERICAL AND EXPERIMENTAL CHARACTERIZATION OF A MULTI-PASS CRYOGENICALLY COOLED Yb^{3+}:CaF_2 LASER AMPLIFIER

Ausgeführt zum Zwecke der Erlangung des akademischen Grades eines Diplomingenieurs

Unter der Leitung von
Univ.Prof. PhD Andrius Baltuška
Univ.Ass Dr.rer.nat. Audrius Pugzlys
PhD Giedrius Andriukaitis
Institut für Photonik

Eingereicht an der Technischen Universität Wien
Fakultät für Elektrotechnik und Informationstechnik

von
Edgar Kaksis,
Matrikelnummer 1227730,

Wien, Mai 2014 _____

Supported by Erasmus Mundus MULTIC Action 2
Partnership Programme

Abstract

Present thesis is dedicated to study and realization of cryogenically cooled solid-state multi-pass (MP) Yb^{3+}:CaF_2 laser amplifier. Within the scope of the thesis specific design questions as active medium choice, thermal behavior of the amplifier, pumping setup, as well as experimental results of the measurements of the amplifier performance will be considered. We have implemented MP scheme seeded by regenerative preamplifier stage and pumped with InGaAs diode laser stack, which can produce up to 200 W average power of pump radiation. Regenerative amplifier, developed during past years in Ultrafast Laser Group at Photonics Institute [Pugzlys, 2009] is capable of delivering up to 10 mJ energy in 500 ps broadband pulses with ~12 nm bandwidth at FWHM. In the framework of this work we aimed to reach 100 mJ output pulse energy at 100 Hz frequency. We provide extensive characterization of implemented MP amplifier, which includes small-signal gain measurement, output energy measurements, output pulse cross-section and spectrum measurements. We address the challenge of beam narrowing during amplification process and offer a solution to resolve it. Achievement of 100 mJ output pulse energy with spectral band of ~12 nm at FWHM at 50 Hz repetition rate is confirmed. We conduct numerical modelling of heat dissipation in the Yb:CaF_2 crystal thermally bonded with blank CaF_2 slabs. Thermal behavior of bonded structure is studied in dependence on the thickness of undoped regions and active area. Heat distribution in the case of double-sided pump is compared to the case of single-sided pump.

Contents

1 Introduction

1.1 Historical overview

From the very beginning of laser era in 1960 laser technology was in continuous pursuit of shorter pulses and higher energies, i.e. trying to achieve higher peak power values. First laser operation in pulsed regime were realized by gain switching and were able to deliver hundred millisecond pulses. The first major achievement on the path of pulse duration reduction became Q-switching method invented in 1962 [Hellwarth, 1962], which allowed obtaining pulses with duration in the order of nanoseconds from ruby laser. Next historical invention followed in 4 years with exploration of passive mode locking technique in 1966 [DeMaria, 1966], which was implemented in Nd-doped glass laser and reduced achievable pulse duration down to 10 ps. Next advancement was reported almost a decade later with appearance of broadband dye active medium combined with dye saturable absorber [Shank, 1974], which produced 1 ps pulses. Persistent refinement of this technique over following years eventually allowed entering sub-picosecond domain. In 1987, implementation of a ring cavity in combination with a prism pair compensating intra-cavity dispersion [Fork, 1987], demonstrated sequences of 6 fs pulses. Several groundbreaking inventions that came in the past several decades superseded the wide use of mode-locked dye lasers in pursuit of shorter pulse durations. In 1990s Ti:Sapphire lasers [Moulton, 1986] were introduced and featured exceptionally broadband gain medium. This stimulated rapid development of chirped pulse amplification technique (CPA) [Strickland, 1985], which nowadays is widely used for producing high-energy ultrashort pulses. Further substantial contribution to the field of ultrashort pulse technology is made by Kerr-lens mode-locking (KLM) technique [Spence, 1991], which allows obtaining pulses as short as 5 fs from Ti:sapphire oscillators, which approaches single-cycle duration limit. Nowadays, broadband solid-

state media along with CPA technique substitute the most successful approach for generation and efficient amplification of ultrashort pulses.

1.1 Motivation

Femtosecond pulses are strongly demanded for numerous cutting-edge applications, such as terahertz radiation generation and sampling or optical parametric chirped pulse amplification (OPCPA). For these and many other fields of optical science the task of producing high-energy pulses with duration in the range of femtoseconds at high repetition rates is of high importance.

1.1.1 Terahertz applications

Terahertz frequency range lies between the optical and microwave regions, and is commonly defined from 0.1 THz to 30 THz [Lee, 2009]. This range used to be called *terahertz gap* (Fig. 2.1) for the reason that until recent times there were no available sources of THz radiation.

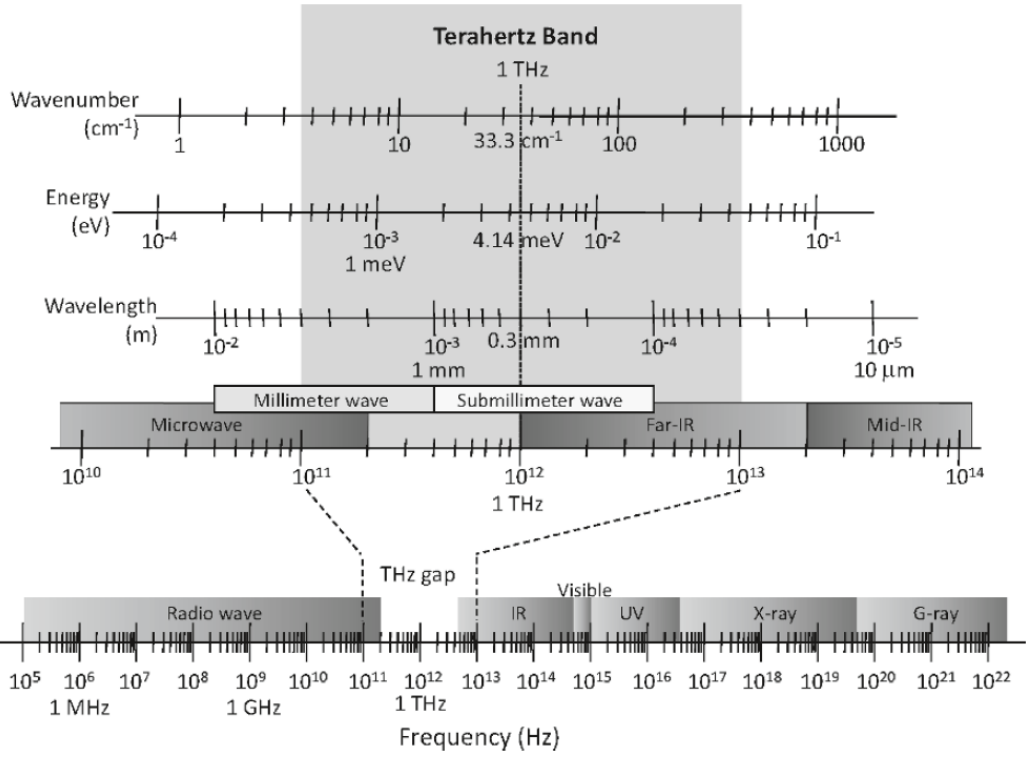

Fig. 2.1 Terahertz band in electromagnetic spectrum [Lee, 2009]

THz radiation is very demanded in many spectroscopic and imaging applications since offers numerous useful features [Zhang, 2010]:

- Many materials consisting of non-polar molecules are transparent in THz frequency range (for example, clays, wood, carton and many others);

- Explosives, drugs, polluting substances, proteins, DNA have distinctive fingerprints in THz region;

- THz radiation is non-ionizing (unlike X-Rays);

- THz wavelengths are relatively long and thus T-rays suffer weak scattering.

One of the commonly used ways for producing THz radiation is *optical rectification* (OR) [Hoffmann, 2011], schematically shown in fig. 2.2.

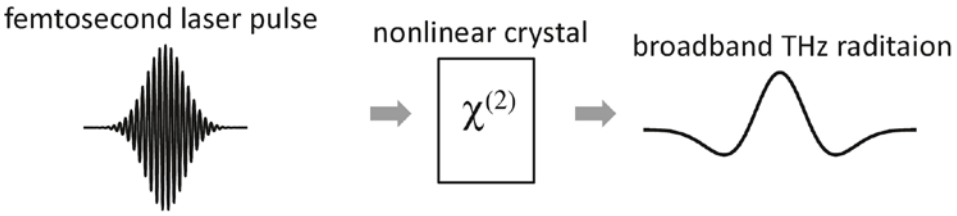

Fig. 2.2 Optical rectification scheme [Lee, 2009]

OR is a second order nonlinear process, based on intrapulse difference frequency generation (DFG), i.e. DFG between different spectral components of a single ultrashort pump pulse. The induced nonlinear polarization in the frequency domain writes as follows [Vodopyanov, 2006]:

$$P_{NL}(\Omega) = \varepsilon_0 \chi^{(2)} \int_0^\infty E(\omega+\Omega) E^*(\omega) d\omega, \qquad \textbf{(2.1)}$$

where ε_0 is the free space dielectric permittivity, $\chi^{(2)}$ is the second-order nonlinear susceptibility of the medium, $E(\omega)$ is the pump spectrum (one-sided Fourier-component), ω is the optical frequency of the pump, Ω is the THz frequency.

Temporal evolution of nonlinear polarization is obtainable by applying Fourier transform:

$$P_{NL}(t) = 2\int_0^\infty P_{NL}(\Omega) \exp[-i\Omega t] d\Omega, \qquad \textbf{(2.2)}$$

where t is the time, $P_{NL}(t)$ is the temporal evolution of nonlinear polarization.

Irradiated THz field is proportional to the second temporal derivative of the polarization:

$$E_{THz}(t) \propto \frac{\partial^2}{\partial t^2} P_{NL}(t), \qquad \textbf{(2.3)}$$

where $E_{THz}(t)$ is the temporal evolution of THz electric field.

The highest THz energies and field intensities in few-THz range are currently achieved with OR techniques in $LiNbO_3$ (LN) crystals [Fülöp, 2011].

As it can be seen from equations above, THz frequency scales with the bandwidth of the pump pulse [Hoffmann, 2011]. It has also been shown that variation of the pump pulse duration not only influences THz frequency, but also modifies pump-to-THz conversion efficiency. The Fourier limited pulse duration of the pump pulse can be tuned in order to utilize the crystal length more efficiently [Fülöp, 2011]. Therefore, ultrashort pulse pump sources are highly demanded by novel THz generation techniques and applications.

The challenge of high THz field generation is stipulated by the low efficiency of optical-to-THz energy conversion [Zhang, 2010]. Recent works show generation of single-cycle 50 μJ THz pulses by OR in LN crystals pumped with multi-mJ pulses from Ti:Sapphire amplifier systems [Stepanov, 2008; 2010]. However, for numerous cutting-edge applications, such as investigation of material properties and processes under the influence of extremely high quasi-static fields, THz-assisted attosecond pulse generation and particle acceleration by electromagnetic waves [Hong, 2009; Bahlog, 2010] THz pulses with energy in mJ range and electric field intensities at 100 MV/cm level are required [Fülöp, 2011]. In order to achieve sufficiently high THz energy levels, pump pulse energy should be increased to 100-mJ level [Fülöp, 2011], which builds motivation for development of high-energy ultrashort pulse sources.

1.1.2 OPCPA pump system

In 2011 our Institute reported the development of Nd:YAG pumped multistage OPCPA system (fig. 2.3), which currently delivers more than 20 mJ output pulse energy in 80 fs pulses centered at 3.9 um at 20 Hz repetition rate [Andriukaitis, 2011]. This system is unique and has recently attracted other research groups to our Institute to collaborate. Several discoveries resulted from these collaborations were reported, e.g. an ultra-broad supecrontinuum in deep UV spectral region produced by high-harmonic generation has been achieved [Popmintchev, 2012]. Free-space nitrogen gas laser driven by a femtosecond filament has been reported [Kartashov, 2012]. Laser induced backward Raman scattering has been investigated [Malevich, 2012].

In the multistage system flash lamp pumped Nd:YAG laser is employed to pump the OPCPA stage (see left upper corner in fig. 2.3). This technology is relatively old and has a substantial drawback of a large quantum defect (2.4) of Nd:YAG gain medium.

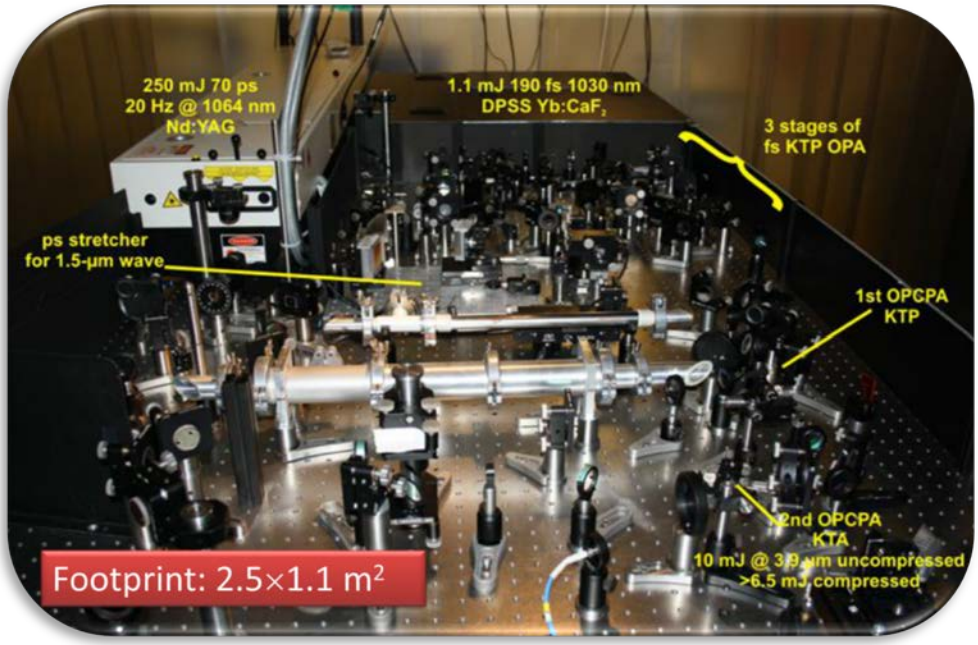

Fig. 2.3 Nd:YAG pumped OPCPA stage [Andriukaitis, 2011]

$$\eta_h = 1 - \frac{\lambda_p}{\lambda_L}, \tag{2.3}$$

where λ_p is the pump wavelength, λ_L is the laser wavelength.

Nd:YAG has a quantum defect of ~34%, which leads to undesirable heat dissipation of substantial amount of pump energy in the laser crystal and eventually limits the obtainable repetition rate.

In order to achieve higher signal-to-noise ratio values of the measurements and to decrease their acquisition time, repetition rates higher than 20 Hz are desirable.

Therefore, we aimed in our work to build a system that would have high enough output pulse energy for high-energy THz generation and high repetition rate in order to replace the pump module of the OPCPA system.

Our ultimate goal is to build a MP amplifier that delivers 100 mJ pulses at a repetition rate of 100 Hz.

Within the scope of this thesis, a design of cryogenically cooled multi-pass amplifier based on Yb^{3+}-doped CaF_2 will be discussed and results of its characterization will be presented.

The subject of the thesis is related to high-energy ultrashort pulse amplification, therefore this work starts with brief description of the principles of laser amplification. In following, various solid-state active media are considered and justification for use of Yb-doped mediums is provided. Especially underlined specific detail here is thermal behavior

of solid-state active media, which is remarkable and advantageous. Afterwards, the design of multi-pass amplifier is considered, starting with the questions of pumping module based on laser diodes, particularly the problem of double-pass geometry realization is addressed, as well as the problem of emission line drift with increase of driving current. General description of used pumping arrangement is given.

Furthermore, the design of multi-pass amplification scheme is discussed. Within the discussion, feasibility of double-stage amplification is established, geometry of amplifier assembled on the optical table is presented, as well as preliminary characterization of amplifier performance, including small-signal gain measurements, spectrum, energy and profile of output beam. The specific problem of beam narrowing in MP setup is addressed. The approaches to overcome this challenge are considered and way to control beam diameter is offered.

Thermal behavior of advanced bonded crystals is numerically simulated. Influence of various parameters on thermal gradients in the gain medium is investigated.

Finally, conclusions and perspectives for future work are given.

2

Theory of the laser amplification

2.1 The concept of population inversion

2.1.1 Boltzmann's statistics

When a large number of atoms is in thermal equilibrium, the ratio between populations of two energy levels E_1 and E_2 with degeneracies g_1 and g_2, (*degeneracy* g_i is the number of states with the same energy E_i)can be described through Boltzmann's formula:

$$\frac{N_2}{N_1} = \frac{g_2}{g_1}\exp\left(\frac{-(E_2 - E_1)}{kT}\right), \qquad \textbf{(2.1)}$$

where N_1 and N_2 are the number of atoms in the energy states E_1 and E_2 with degeneracies g_1 and g_2, k is the Boltzmann constant, T is the temperature of the system.

Boltzmann's law states that under thermal equilibrium condition the state with a lower energy will be more populated than that with a higher energy, as depicted in fig. 2.1, while at T=0 all the atoms will reside in the ground state [Koechner, 2003].

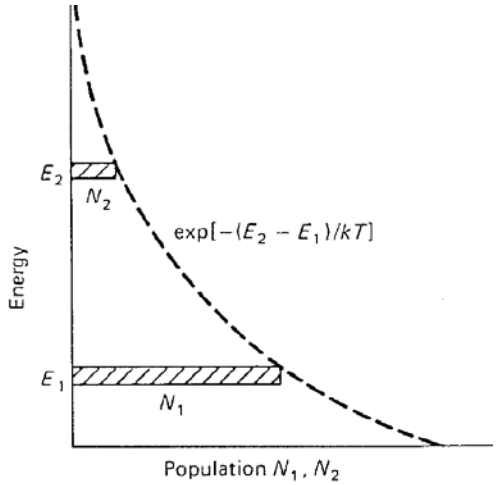

Fig. 2.1 Relative populations of two energy levels according to Boltzmann's statistics in thermal equilibrium

2.1.2 Einstein's coefficients

Consider a simple system with only two non-degenerate energy levels 1 and 2 with populations N_1 and N_2, assuming that the number of atoms of the system remains constant, i.e.:

$$N_1 + N_2 = N_{tot} \quad \textbf{(2.2)}$$

Radiative transfer between the levels 1 and 2 is allowed, i.e. the atom can transfer from energy level E_2 to the state E_1 by emitting energy in the form of a photon:

$$E_2 - E_1 = h\nu_{21}, \quad \textbf{(2.3)}$$

where *h* is the Plank constant, ν_{21} is the frequency of the transition between levels 2 and 1. Alternatively, atom can make transition from level 1 to level 2 by absorbing the same amount of energy. Coefficients A_{21}, B_{21} and B_{12}, introduced by Einstein, characterize spontaneous and induced transitions between these two levels.

If a monochromatic electromagnetic wave with frequency ν_{21} passes through the described system, the population of the lower level will deplete at a rate proportional both to the population N_1 of level 1 and to the radiation density $\rho(\nu)$:

$$\frac{\partial N_1}{\partial t} = -B_{12}\rho(\nu)N_1, \quad \textbf{(2.4)}$$

where B_{12} is the Einstein's coefficient with dimensions cm^3/s^2J. The physical meaning of the product $B_{12}\rho(\nu)$ is the absorption rate, which is proportional to the photon flux:

$$B_{12}\rho(\nu) = \sigma_{12}F = \sigma_{12}\frac{I}{h\nu}, \quad \textbf{(2.5)}$$

where σ_{12} is the absorption cross-section, *F* is the photon flux, *I* is the intensity of the inducing radiation.

After the atoms transited in the higher energy state 2 as a result of the absorption process, the population of the level 2 depletes spontaneously to the state 1 at a rate proportional to the population N_2 of level 2:

$$\frac{\partial N_2}{\partial t} = -A_{21}N_2, \quad \textbf{(2.6)}$$

where A_{21} is the Einstein's coefficient with dimensions s^{-1}. The physical meaning of A_{21} is the probability of spontaneous transition from the level 2 to the level 1.

Spontaneous emission can occur without a presence of the electromagnetic field, and is characterized by the lifetime of the electron in the excited state, which enters the solution of (2.5):

$$N_2(t) = N_2(0)\exp\left(\frac{-t}{\tau_{21}}\right), \quad \textbf{(2.7)}$$

where $N_2(0)$ is the population of level 2 at initial time point, $N_2(t)$ is the population of level 2 after time *t*, τ_{21} is the lifetime of level 2, which is reciprocal of A_{21}.

$$A_{21} = \frac{1}{\tau_{21}}, \quad \textbf{(2.8)}$$

Emission can occur not only spontaneously, but also stimulated by electromagnetic wave at the appropriate frequency. As a result, the atom makes a transition from level 2 to level 1 with emitting a quantum of *induced* radiation, which is described as follows:

$$\frac{\partial N_2}{\partial t} = -B_{21}\rho(\nu)N_2, \quad \textbf{(2.9)}$$

where B_{12} is the Einstein's coefficient for induced emission. The physical meaning of the product $B_{21}\rho(\nu)$ is the stimulated emission rate, which is proportional to the incident photon flux:

$$B_{21}\rho(\nu) = \sigma_{21}F = \sigma_{21}\frac{I}{h\nu}, \quad \textbf{(2.10)}$$

where σ_{21} is the emission cross-section, *F* is the incident photon flux, *I* is the intensity of the stimulating radiation.

Thus, atomic system emits radiation in the presence of external electromagnetic wave, that consists of two parts – spontaneous radiation, whose intensity is proportional to A_{21} and is not phase-related, and induced emission, whose intensity is proportional to $B_{12}\rho(\nu)$ and is coherent to the inducing wave. Summarizing (2.2), (2.4), (2.5) and (2.8), we obtain the relation for the two-level system [Siegman, 1986]:

$$\frac{\partial N_1}{\partial t} = -\frac{\partial N_2}{\partial t} = B_{21}\rho(\nu)N_2 - B_{12}\rho(\nu)N_1 + A_{21}N_2, \quad \textbf{(2.11)}$$

2.1.3 Population inversion

Boltzmann' statistics suggests that at thermal equilibrium higher-energy level is less populated than lower-energy level, as has been discussed before. In this situation, in the presence of electromagnetic radiation of appropriate wavelength, induced absorption will be

observed. If a temporary situation that upper state contains more atoms than the lower state is achieved, than normally positive population difference N_1 - N_2 becomes negative (fig. 2.2).

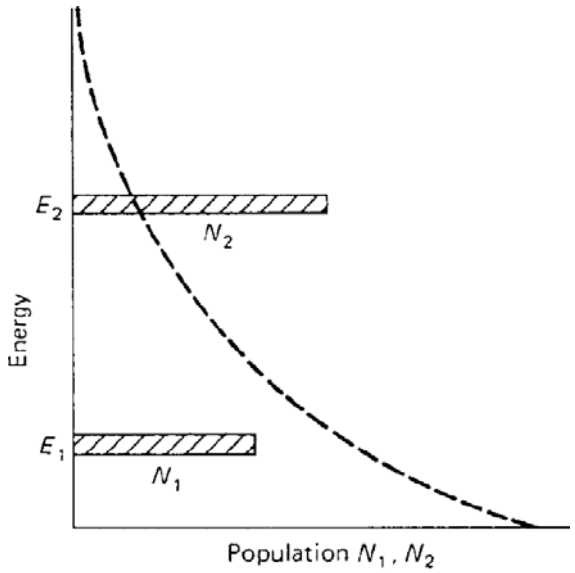

Fig. 2.2 Inverted population inversion [Koechner, 2003]

In this situation propagating electromagnetic wave will induce emission instead of absorption and thus, experience gain. Therefore, the essential condition for amplification in the system is that higher energy level contains more atoms than the lower one [Siegman, 1986]:

$$N_2 > N_1 \text{ if } E_2 > E_1 \qquad \textbf{(2.12)}$$

However, according to Boltzmann's statistic this is never the case in two level system, thus population inversion cannot be achieved in 2-level system. Three- or four energy level system is required.

2.2 Energy level schemes

2.2.1 Three-level system

The three-level system is schematically depicted in fig. 2.3.

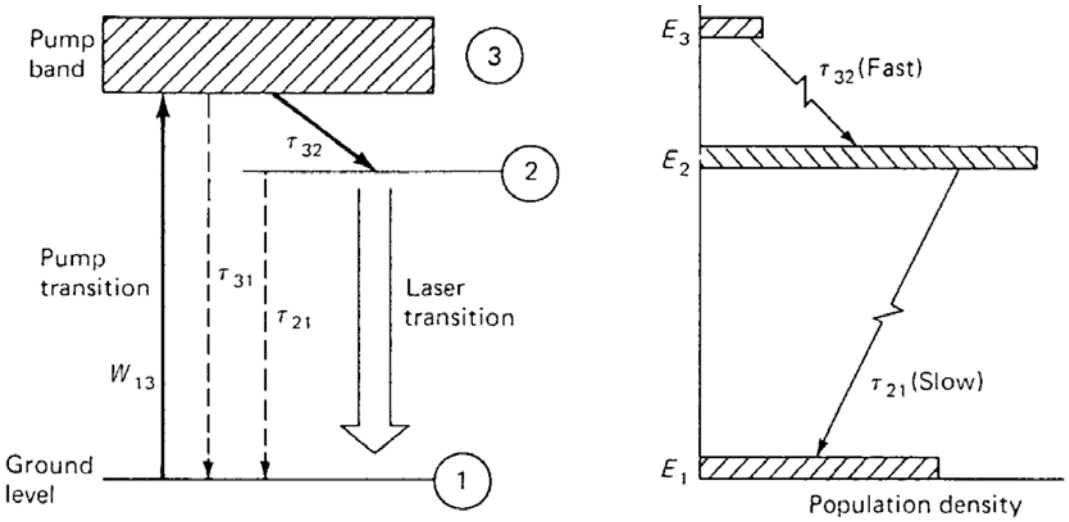

Fig. 2.3 Simplified energy level diagram of a three-level system [Koechner, 2003]

At the initial moment, all ions of the gain medium are in the lowest energy state 1. The excitation into the broad band 3 is realized with inducing (pump) radiation at a wavelength corresponding to the energy gap between levels 1 and 3, which stimulates absorption. Most of the excited ions residing in energy band 3 are transferred by fast radiationless transitions into the level 2. In this process, the energy lost by the electron is transferred to the lattice. Eventually, the atom returns to the ground level 1 by the emission of a photon.

It is important in the three-level system that the lifetime of level 3 is considerably longer than the relaxation time of the transition from band 3 to level 2, i.e. $\tau_{21} >> \tau_{32}$.

The dynamics of the amplification can be described with high precision by a set of coupled rate equations, which represents a pair of simultaneous differential equations that describe the population inversion and the radiation density within a spatially uniform laser medium.

In order to approximate the three-level scheme with a two-level system, we will assume that the transition from the band 3 to the upper laser level is fast enough to neglect population of band 3 (N3 ≈ 0). Therefore, pumping has no influence on radiative processes and only allows populating the upper level and thereby obtaining population inversion (N2 > N1). The system of coupled equations can then be described as follows [Siegman, 1986]:

$$\begin{cases} \dfrac{\partial N_1}{\partial t} = \left(N_2 - \dfrac{g_2}{g_1} N_1 \right) F^{las} \sigma_{21} + \dfrac{N_2}{\tau_{21}} - F^{pump} \sigma_{13} N_1, \\ \dfrac{\partial N_2}{\partial t} = -\dfrac{\partial N_1}{\partial t} \end{cases}, \qquad \textbf{(2.13)}$$

where F^{las} is the flux of stimulating radiation, F^{pump} is the flux of pump radiation.

The terms on the right-hand side in the first equation of (2.13) express the stimulated emission, the spontaneous emission and the pumping [Koechner, 2003].

The drawback of the three-level system is that the optical transitions occur directly on the ground level. Therefore, ground-state absorption (GSA) takes place at the emission wavelength, which deteriorates operation efficiency.

2.2.2 Four-level system

The four-level system is schematically depicted in fig. 2.4.

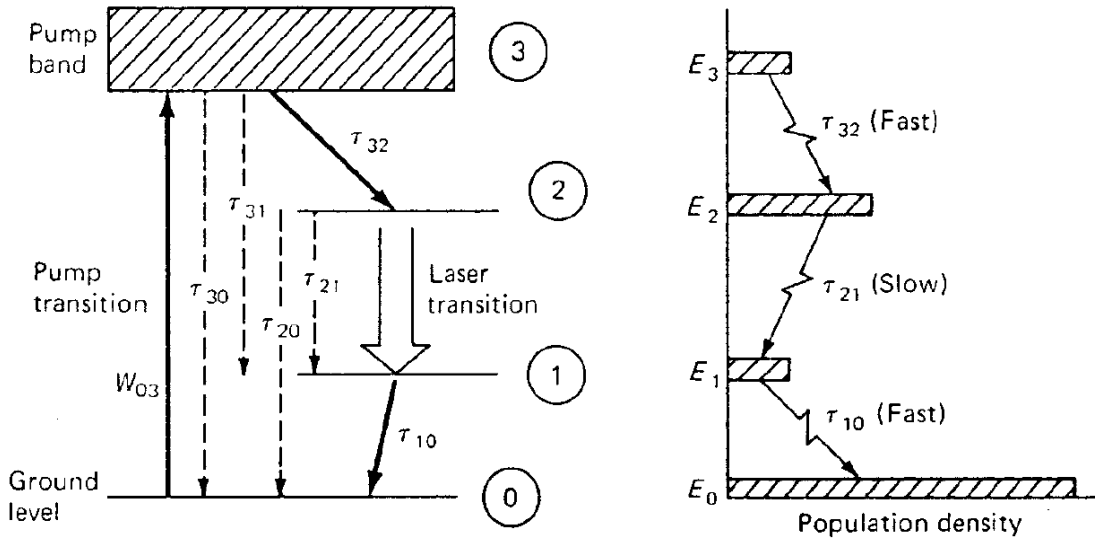

Fig. 2.4 Simplified energy level diagram of a four-level system [Koechner, 2003]

In four-level system we assume again that the transition from the band 3 to the upper laser level 2 occurs rapidly. The system of rate equations for the four-level system writes as follows [Koechner, 2003]:

$$\begin{cases} \dfrac{\partial N_2}{\partial t} = F^{pump} \sigma_{03} N_g - \left(N_2 - \dfrac{g_2}{g_1} N_1 \right) F^{las} \sigma_{21} - \left(\dfrac{N_2}{\tau_{21}} + \dfrac{N_2}{\tau_{20}} \right), \\ \dfrac{\partial N_1}{\partial t} = \left(N_2 - \dfrac{g_2}{g_1} N_1 \right) F^{las} \sigma_{21} + \dfrac{N_2}{\tau_{21}} - \dfrac{N_1}{\tau_{10}}, \\ N_{tot} = N_g + N_1 + N_2 \end{cases}, \qquad \textbf{(2.14)}$$

where N_g is the population of the ground level 0, σ_{ij} are the cross-sections of *i->j* transitions.

It can be seen from fig. 2.4 that the population of the upper laser level 3 of a four-level system increases due to pumping and decreases because of stimulated emission and spontaneous emissions to levels 0 and 1. The lower level population increases because of spontaneous and stimulated emissions and decreases due to radiationless relaxation process into the ground level 0. This process is characterized by the time constant τ_{10}. In an ideal four-level system the terminal level 1 empties rapidly to the ground level 0. If we accept $\tau_{10} \approx 0$, then $N_1 = 0$, which follows from the second equation in (2.14). In this case the entire population is distributed between the ground level 0 and the upper level 2 of the laser transition. Having assumed this, we obtain the following rate equation for the ideal four-level system:

$$\frac{\partial N_2}{\partial t} = F^{pump}\sigma_{03}\left(N_g - N_2\right) - N_2 F^{las}\sigma_{21} - \frac{N_2}{\tau_f}, \qquad \textbf{(2.15)}$$

where τ_f is the fluorescence decay time of the upper laser level 2:

$$\frac{1}{\tau_f} = \frac{1}{\tau_{21}} + \frac{1}{\tau_{20}} \qquad \textbf{(2.16)}$$

Thus, in a four-level system, the lower laser level 1 lies above the ground state 0. Since the number of thermally excited atoms in the lower laser level 1 is small, the population can be inverted by pumping a small number of atoms into the upper laser level 2 easily. Therefore a four-level scheme requires less energy to create a population inversion compared to a three-level system. The parasitic GSA in four-level system is efficiently suppressed, which gives the four-level scheme substantial advantage over the three-level scheme.

2.3 Small-signal regime

The small-signal gain of the active medium is the gain obtained for an input signal which is sufficiently weak that it does not cause any gain saturation [Paschotta, 2008].

As long as the intensity $I(z)$ of the amplified radiation is substantially small so that it does not significantly deplete population inversion, it can be described by the following differential equation:

$$\frac{dI}{dz} = \sigma_{21}(\nu)\Delta N_{21} I(z), \qquad \textbf{(2.17)}$$

where $I(z)$ is the intensity distribution along the propagation direction z, ΔN_{21} is the population inversion between the upper laser level 2 and the lower laser level 1. The term of small-signal gain can be introduced:

$$g_0(\nu) = \sigma_{21}(\nu)\Delta N_{21}, \qquad \textbf{(2.18)}$$

Therefore, the differential equation (2.17) can be solved and gives exponentially growing function as a result:

$$I(z) = I_{in} \exp\left(g_0(\nu) z\right), \qquad \textbf{(2.19)}$$

where I_{in} is the input radiation intensity for z=0.

As it can be seen from (2.19), the output intensity of the amplifier in non-saturated mode scales linearly with seed intensity. At high seed intensities this is not valid anymore.

2.4 Amplification of high-energy pulses

2.4.1 Gain saturation

The gain medium of the amplifier cannot maintain fixed gain value for arbitrarily high input powers, since it would require adding arbitrary amounts of power to the amplified signal. Thus, the gain must be reduced for high input powers; this phenomenon is called *gain saturation* [Paschotta, 2008]. In the steady state and under assumption of not saturated pumping can be described as follows:

$$g = \frac{g_0}{1 + \frac{I}{I_{sat}}}, \qquad \textbf{(2.20)}$$

where I_{sat} is the saturation absorption $I_{sat} = \frac{h\nu}{\sigma_{21}(\nu)\tau_{sat}}$, where τ_{sat} is the saturation time constant [Siegman, 1986]. At the radiation intensity equal to saturation intensity, gain drops by the factor of two, as depicted in fig. 2.5.

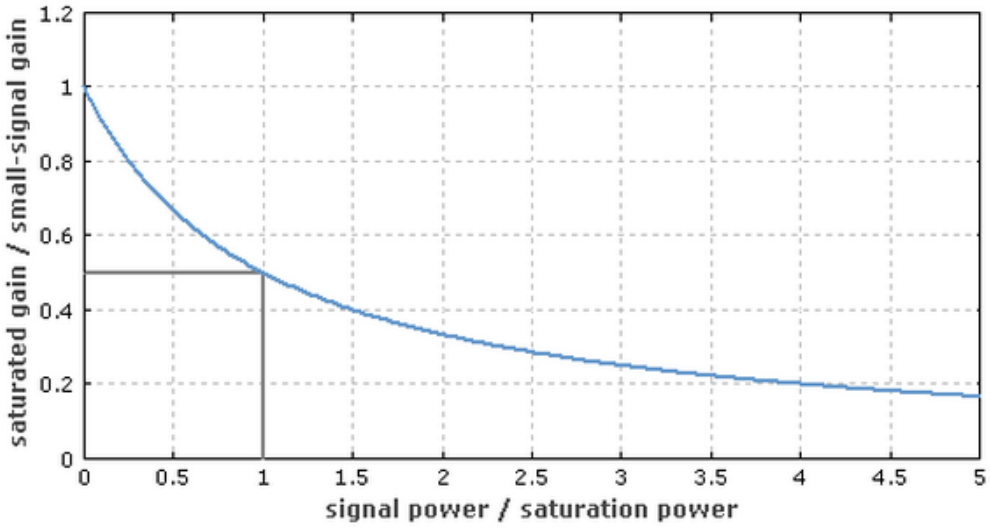

Fig. 2.5 Dependence of the saturated gain on the signal power in the steady state [Paschotta, 2008]

In the case of short pulse amplification, saturation influences the gain more drastically. The effective gain that the pulse experiences is some averaged value, since the gain decreases during the amplification process. This average gain value can be calculated by considering the reduction of the stored energy in the gain medium. In the simpler case, where the gain is small, so that the intensity is approximately constant within the amplifier, it can be calculated as follows:

$$g_{pulse} = g_0 \frac{E_{sat}}{E_{pulse}} \left(1 - \exp\left(-\frac{E_{pulse}}{E_{sat}} \right) \right), \qquad \textbf{(2.21)}$$

where E_{pulse} is the pulse energy, E_{sat} is the saturation energy, g_0 is the unsaturated gain coefficient. This dependence is presented in fig. 2.6.

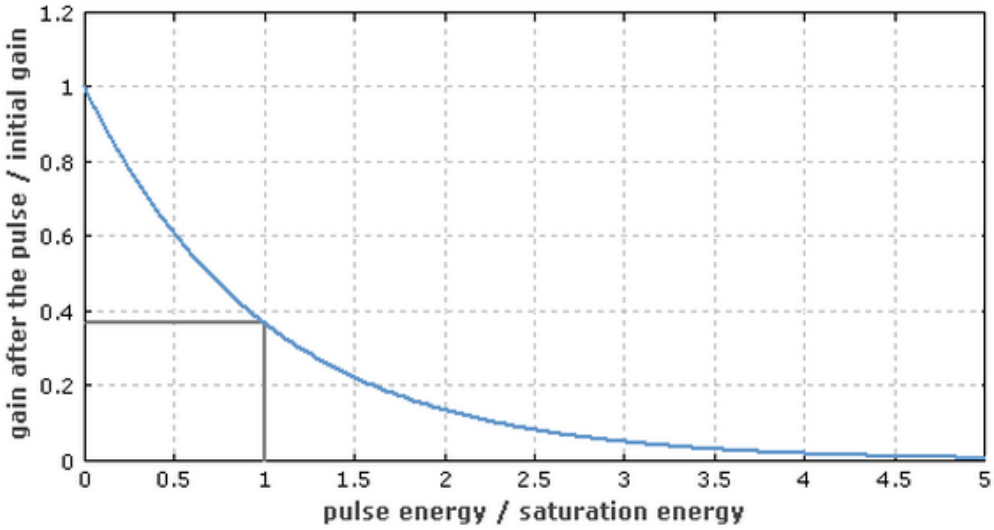

Fig. 2.5 Dependence of the saturated gain on the pulse energy in the pulsed mode [Paschotta, 2008]

In the more general case with arbitrarily high gain, the *Frantz-Nodvick equation* should be used:

$$g_{pulse} E_{out} = E_{sat} \ln\left[1 + \exp(g_0) \left(\exp\left(\frac{E_{in}}{E_{sat}} \right) - 1 \right) \right] - \left(1 - \exp\left(-\frac{E_{pulse}}{E_{sat}} \right) \right), \qquad \textbf{(2.22)}$$

2.4.2 Homogeneous and inhomogeneous saturation

There are two distinctive natures of gain saturation. Homogeneous gain saturation means that the spectral curve of the gain is not influenced by the saturation. This takes place e.g. when all active ions have the same emission spectrum. In some gain media, particularly in disordered media the active ions can occupy different sites in the lattice, thus the differing local electric fields affect the wavelengths and strength of the different transitions. This can lead to inhomogeneous saturation, so that the gain around the laser wavelength is saturated more than the gain at other wavelengths, which is depicted in fig. 2.6 [Paschotta, 2008].

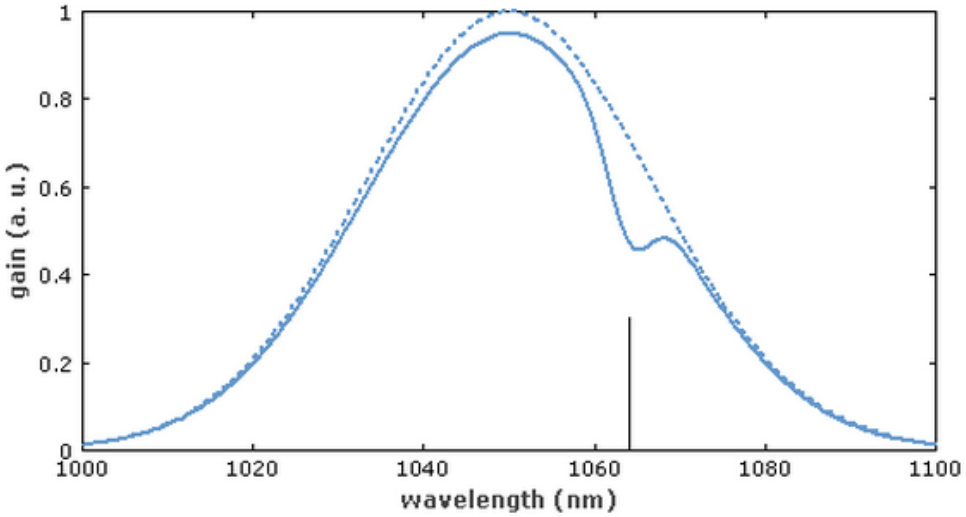

Fig. 2.6 Example of inhomogeneous gain saturation at 1064 nm. Dashed line represents unsaturated gain curve [Paschotta, 2008]

2.4 CPA concept

Chirped pulse amplification [Strickland, 1985] is the method to amplify ultrashort pulses that is widely used in modern ultrashort pulse applications. Its motivation consists in the problem that ultrashort pulse creates significant intensity in solid-state amplifier gain medium, which can easily exceed optical damage threshold of the material. The idea of CPA is to maintain energy contained in the ultrashort pulse while decreasing the intensity that it creates in the laser crystal by stretching the pulse in time domain. After amplification of the stretched pulse in the gain medium, the pulse is compressed back to its initial duration by compressor system. This technique allows obtaining extreme power levels up to petawatts [Paschotta, 2008]. The principal CPA scheme is depicted in fig. 2.6.

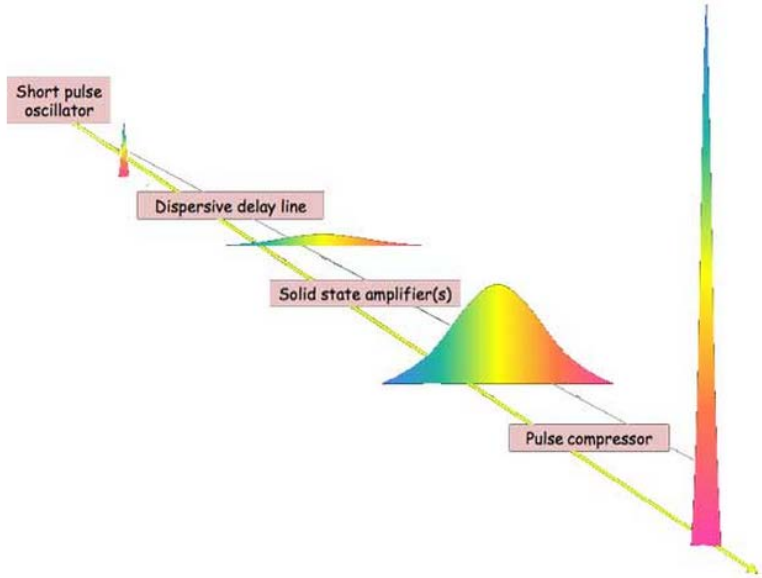

Fig. 2.6 CPA principal scheme [Nev.TW Facility]

As a stretcher and compressor stages, different dispersive schemes can be implemented; the essential requirement is that dispersion introduced by the compressor is opposite in sign to that of the stretcher and equal by the absolute value.

Initially, optical fiber has been used to stretch the pulse providing positive GDD with following compression by two parallel diffraction gratings [Treacy, 1969]. The best dispersive characteristics belong to the grating-based systems and allow efficient stretching in compact constructions.

Having briefly observed theoretical aspects of laser amplification, we will consider particularly the design of the cryogenically cooled MP amplifier for chirped ultrashort pulses.

3

Gain media of CPA system

3.1 Gain medium requirements for chirped pulse amplification

The primary task in the development of an amplifier for ultrashort pulses is the choice of the gain media appropriate for the application. Gain media properties determine the central wavelength, absorption and emission cross-sections and saturation intensities, achievable bandwidth and thus output pulse duration. It also determines quantum defect of the active media, hence efficiency of energy extraction and amount of heat dissipated in the laser crystal, while thermal conductivity of active medium influences the quality of the output beam.

In the field of ultrashort pulse amplification one of the soundest requirements is *broad gain bandwidth*, since it allows amplification of broadband pulses. *High thermal conductivity* is essential to suppress undesirable thermal effects such as thermally induced birefringence, thermal lensing and crystal damage that are especially severe in high average power systems. Higher thermal conductivity provides lower thermal gradients and eases thermal stresses and their consequences. *High absorption cross-section* is needed to provide efficient use of pump radiation, while *high emission cross-section* gives the advantage in numerous aspects:

- high small-signal gain coefficient, $$\gamma(\nu) = \sigma_{em}(\nu) \cdot \Delta N_{21} \quad \textbf{(3.1)}$$
- low saturation fluence, $$F_{sat}(\nu) = \frac{h\nu}{\sigma_{em}(\nu)} \quad \textbf{(3.2)}$$
- low pump intensity threshold, $$I_{th}^{pump}(\nu) = \frac{h\nu}{\sigma_{em}(\nu)\tau} \cdot \frac{\nu^{pump}}{\nu} \cdot \frac{\alpha_{loss}}{\alpha_{pump}}, \quad \textbf{(3.3)}$$

where $\sigma_{em}(\nu)$ is the spectral distribution of the emission cross-section, ΔN_{21} is the population inversion, h is the Plank constant, ν is the lasing frequency, τ is the radiative lifetime, ν^{pump} is the pump frequency, α_{loss} is the absorption coefficient at the laser wavelength, α_{pump} absorption coefficient of the pump.

Besides, the absorption line of active medium should match the emission line of available pump sources. *Long upper level lifetime* is required to provide efficient storage of population inversion. Additionally, it influences the dynamics of population inversion. If lifetime is longer than the inverse repetition rate then cw pump can be employed, while in case of long pulse periods pulsed pump is needed.

3.2 Various active ions

Active medium of DPSS amplifier can employ different active ions, which possess diverse properties appropriate for various applications. In general, two groups of active ions can be marked out, namely *transition-metal ions* and *rare-earth ions*. In case of transition-metal ions, optical transitions occur in the outer 3d-shell and have vibronic nature [Koechner, 2003]. Active media based on TM ions offer broad absorption and emission bandwidth.

One of the pioneering and most popular throughout last decades TM ion based solid-state lasers (SSL) that can work in spectral region around 0.8 um is Ti^{3+}:sapphire. Due to its large bandwidth, this gain medium supports very short pulse duration down to a single optical cycle duration and excellent spectral tunability in the range from 670 to 1100 nm. It also offers exceptionally good thermal conductivity of 33 W/(m*K) [Gulevich, 1994] that allows efficient mitigation of undesired thermal effects, as well as relatively high emission cross section. One of major problems of titanium-sapphire laser systems is that their gain medium has absorption region lying around green wavelengths (~500 nm, fig. 3.3 [Koechner, 2003]), where no powerful laser diode pumping systems are available, hence expensive and complicated laser system should be employed for pumping (e.g. SH Nd:YAG or Ar-ion laser).

Another laser ion active in the vicinity of 1 um is Nd^{3+}, which belongs to the group of lanthanide rare-earth elements. Electronic configuration of Nd^{3+} is [filled 1s..4d shells] $4f^3 5s^2 5p^6$. Optical transitions occur inside the 4f shell, which is screened by 5s and 5p shells, therefore crystalline field of hosting crystal does not severely affect spectroscopic properties of Nd^{3+} ions. Most commonly, Nd^{3+} ions are incorporated in oxides and fluorides. Characteristic feature of Nd-doped media is high emission cross-section and thus high single-pass gain. Emission line of Nd^{3+} doped crystals is relatively narrow. This makes them inappropriate for ultra-short pulse generation and amplification purposes.

During recent years, Yb-doped laser materials have received particular appreciation as active medium for high-energy ultra-short pulse amplification. Yb^{3+} active media have closely spaced absorption and emission lines, namely ~976 nm and ~1030 nm respectively, which on the one hand allows effective pumping, since absorption line matches emission line of powerful InGaAs laser diodes, and on the other hand implies low quantum defect (2.3) due to small Stokes shift between the emission and absorption lines.

This gives a significant advantage of lower thermal load of the crystal, since smaller amount of absorbed energy is dissipated as a heat.

Energy level diagram, of Yb^{3+} consists of two broadened levels, lower $^2F_{7/2}$ and excited state $^2F_{5/2}$, separated by approximately 10000 cm^{-1}.

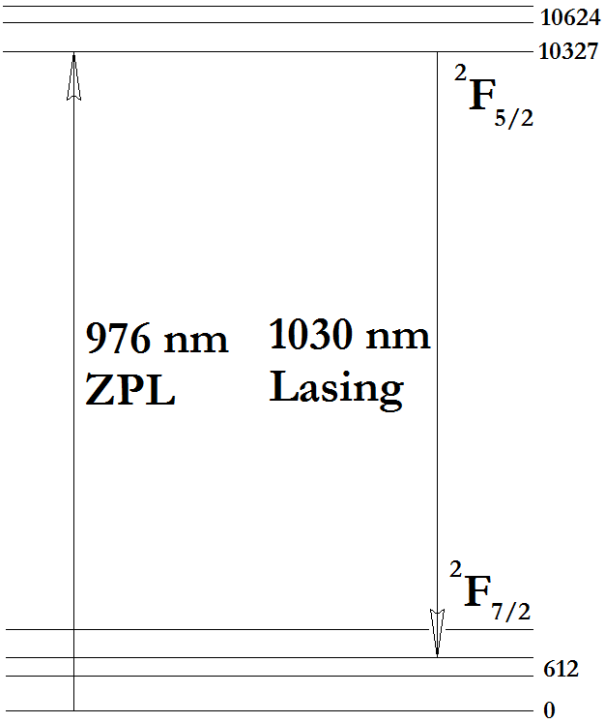

Fig. 3.1 Laser level system of Yb^{3+}

Thermal energy at room temperature (RT) is kT = 200 cm^{-1}, where k = 1.3806488×10^{-23} J/K is the Boltzmann's constant, therefore Yb^{3+} possess quasi-three-level system with around 5.5% thermal population of the lower laser level at RT [Koechner, 2003]. However, when cooled, Yb-doped material transforms to four-level system, which will be discussed later. These properties make Yb-doped materials interesting for high average power ultra-short pulse applications. In following, behavior of Yb^{3+} ion in various crystalline environments will be discussed.

3.3 Properties of Yb^{3+}-doped active media

Crystalline host, in which Yb^{3+} ions are incorporated, influences mechanical, thermal and spectroscopic properties of gain media substantially. Wide spread hosts for Yb^{3+}-doped medium are various oxides (e.g. garnets, sapphire, and ruby), silicates, phosphates, fluorides (e.g. YLF, CaF_2), chlorides, bromides, tungstates. Table 1 summarizes properties of different Yb^{3+}-doped crystals.

Table 1. Properties of Yb^{3+}-doped active media

Group	Material	Bandwidth, nm	σ_{em}, peak 10^{-20} cm^2	σ_{abs}, peak 10^{-20} cm^2	Lifetime τ, ms	Thermal conductivity κ (undoped), W/m/K
Fluoride	Yb:CaF_2	80	0.17-0.2	0.54	2.4	9.7
Fluoride	Yb:SrF_2	72	0.15	0.91	2.9	8.9
Aluminate	Yb:YAG	6.3-8.5	2.1	0.83	0.95	8.6-11
Sesquioxide	Yb:Y_20_3	12.2	1.1	0.24	0.85	13.6
Borate	Yb:BOYS	60	0.2	0.8	1.1	1.4-1.8
Tungstate	Yb:KGW	20-25	2.8	12	0.6	3.3
Silicate	Yb:SYS	73	0.4	0.4	1.1	2.8
Glass	Yb:glass	52	0.64	2.6	0.8	0.6-0.8

Yb^{3+}-doped aluminates, for instance [Honn, 99; Aggr, 05; Brenn, 01], have relatively large emission cross-section and good thermal conductivity, which in combination makes them promising media for extracting high peak and average powers. However, due to regular structure of the crystal, they have narrow gain bandwidth, which restricts the obtainable pulse duration to 680 fs [Russ, 09]. Yb-doped aluminates are thus suitable for sub-picosecond high power applications.

On the contrary, Yb^{3+}-doped borates have a very broad gain band [Honn, 99; Druo, 02] and allow generating and amplifying ultrashort pulses with duration as short as 69 fs [Druo, 02]. On the other hand, borates have small emission cross-section and poorly conduct heat. Thus, they are good for low power ultrashort pulses applications.

Properties similar to that of aluminates are also typical for sesquioxides, in which relatively high emission cross-section and high thermal conductivity is combined with narrow emission band. Thus, Yb^{3+}-doped sesquioxides are also applicable in the field of high-power amplification of picosecond pulses. Moreover, another complication in the

case of sesquioxides relates is strict requirements for the crystal growth, which makes it difficult to produce such crystals.

Yb^{3+}-doped tungstates distinguish themselves through moderate bandwidth and relatively high emission cross-section. However, they also have several drawbacks, such as short upper state lifetime, which determines low energy storage capacity of such media, relatively low thermal conductivity, which restricts obtainable power, and high nonlinear Raman susceptibility [Laga, 00].

Both silicates and glasses doped with Yb^{3+} ions have broad gain bandwidth; hence, can support ultrashort pulse generation and amplification. Nevertheless, apart from this advantage they offer small emission cross-section, short lifetime of the upper state and low thermal conductivity.

Especially interesting from the point of view of high-energy and high average power ultrashort pulse amplifiers laser materials are Yb-doped fluorides. They possess following remarkable properties:

- Transparency in a wide spectral range from deep UV up to IR;
- Low linear and nonlinear refractive indices;
- Low non-radiative relaxation rate between adjacent energy levels;
- Relatively broad gain bandwidth;
- Long radiative lifetime;
- High thermal conductivity.

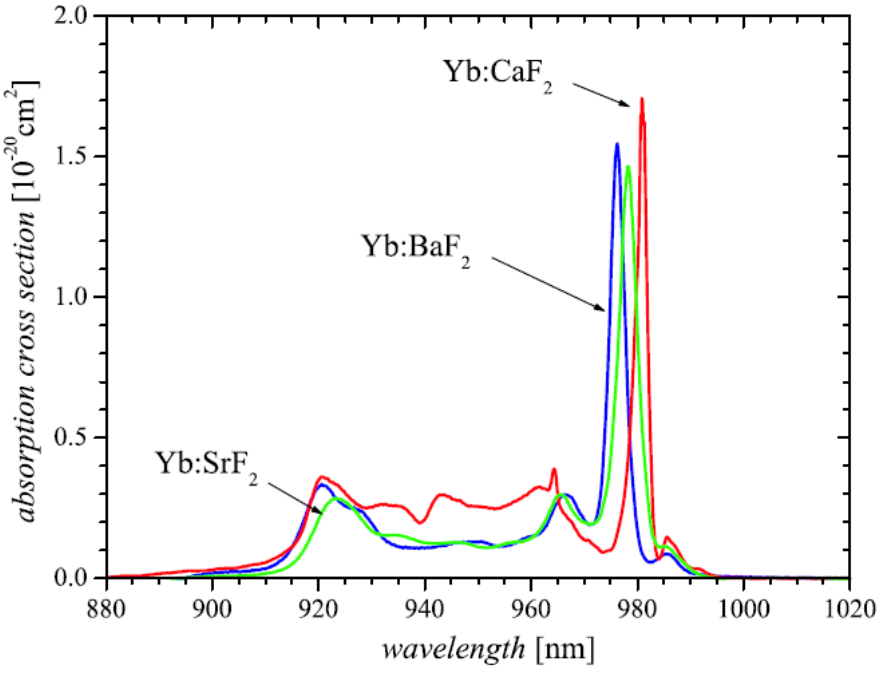

Fig. 3.2 Absorption cross-section spectra of Yb^{3+} ions in different fluoride hosts at 77 K [Siebold, 2009]

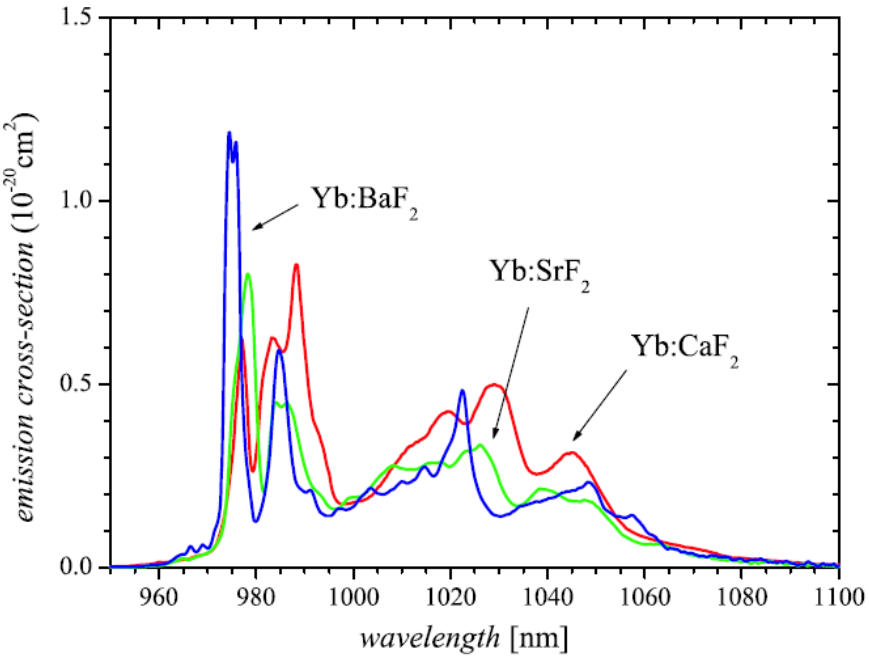

Fig. 3.3 Emission cross-section spectra of Yb^{3+} ions in different hosts [Siebold, 2009]

Gain bandwidth of the laser crystal is a crucial parameter for ultrashort pulse generation and amplification, and Yb^{3+}-doped fluoride crystals possess the broadest gain bandwidths among others, as it follows from table 1. This broad gain bandwidth is stipulated by the clusterization of Yb^{3+} ions at high doping concentrations in hexameric clusters [Siebold, 2009]. Yb^{3+}-doped fluorides have relatively small emission cross-section [Siebold, 2009; Chen, 01; Ueha, 96; Kawa, 02; Lucc, 04; Ito, 04; Druo, 09; Boud, 08]. Small values of the emission cross-section leads to high saturation intensity and to low single-pass gain (3.1, 3.2). As a result, efficient energy extraction requires high seed intensities, which implies tight focusing into the crystal.

Lifetime of the upper level of gain medium determines the energy storage capacity; active media with longer lifetimes allow obtaining capacious energy storages. In the case of Yb^{3+}-doped media, distinctive influence on the lifetime of the upper state has a crystal field of the host since Yb^{3+} possesses weak screening of 4*f* electrons by 5*s* and 5*p* shells [Laga, 00]. When incorporated into crystals with central symmetry, Yb^{3+} ion is least influenced by crystalline field and thus can remain in the excited state longer.

From this consideration follows that Yb^{3+}-doped fluorides represent the optimal active media for high-energy ultrafast amplifiers, among which Yb^{3+}:CaF_2 exhibits the best combination of relevant mechanical, optical and thermal properties, which can be further improved by the thermal management of active medium.

3.4 Temperature dependent properties of Yb^{3+}:CaF_2

It is well known that performance of solid-state active medium strongly depends on the operation temperature. In the case of Yb^{3+}-doped calcium fluoride, thermal influence is distinctive in several aspects.

Firstly, at room temperature Yb^{3+}:CaF_2 operates in a quasi-three-level energy scheme. This results in stronger ground state absorption (GSA) and higher laser threshold and therefore limits reachable gain. Cryogenic cooling reduces thermal broadening of the energy levels and thus transforms the energy scheme of the active medium to a four-level scheme, which allows achieving higher gain and efficiency.

Secondly, Yb^{3+}:CaF_2 possess moderate emission cross-section at RT, which implies small single-pass gain. This is not desirable in high-energy amplifiers since requires more passes through the active medium for efficient amplification, while each pass leads to degradation of the beam quality through thermo-optical distortions and gain narrowing effects. At cryogenic temperatures the emission cross-section increases substantially [Pugzlys, 2009], as it can be seen from fig. 3.9, from ~$1.9*10^{-21}$ cm^2 at 1030 nm at 300 K to $3.4*10^{-21}$ cm^2 at 110 K. Thus, single-pass gain (3.1) almost doubles and saturation intensity decreases.

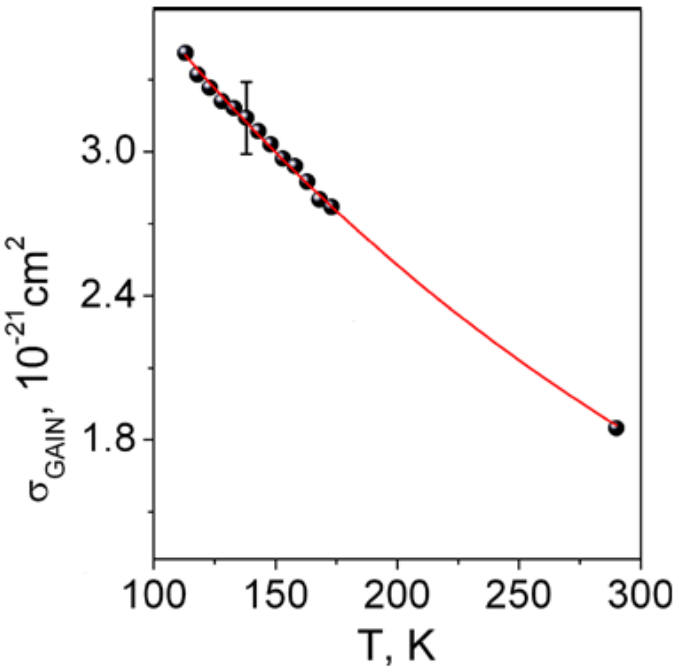

Fig. 3.4 Dependence of gain cross-section for the 2%Yb, <0.1%Na codoped CaF_2 crystal at 1030 nm on temperature [Pugzlys, 2009]

Besides, absorption cross-section increases at low temperatures as well [Boud, 08]. While at RT at zero-phonon line (ZPL) of 976 nm it equals ~0.59*10^{-20} cm^2, at 77 K absorption cross-section at ZPL rises up to 1.57*10^{-20} cm^2 [Siebold, 2009], as depicted in fig. 3.5. As a result, pump absorption increases, which allows efficient pump use in only one or two pump beam passes through active medium.

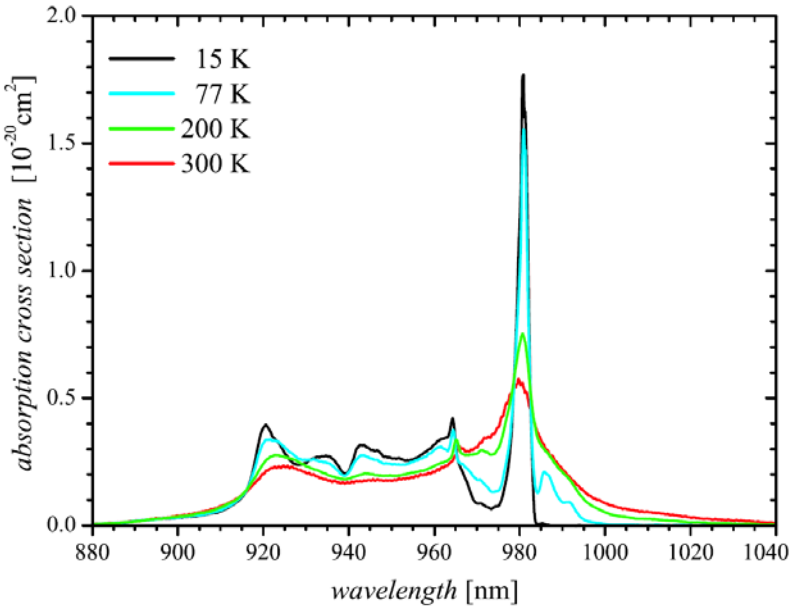

Fig. 3.5 Absorption cross-section spectrum of a 4.5% Yb^{3+}:CaF_2 crystal at various temperatures [Siebold, 2009]

Moreover, cryogenic cooling strongly influences thermal properties of the active medium. Undoped CaF_2 at RT has thermal expansion coefficient of 19*10^{-6} K^{-1}, thermal shock parameter of 0.18 kWm^{-1}, thermo-optical coefficient of -17.8*10^{-6} K^{-1} and thermal conductivity of 9.7 W/m/K. Cryogenic cooling improves these parameters significantly, e.g. the thermal expansion coefficient decreases by a factor of 4.2, the thermo-optic coefficient scales down by 3.6 and the thermal conductivity increases by a factor of 7 [Slack, 1961; Boudeile, 2008; Ladison, 2005; Druon, 2011].

Nevertheless, such outstanding thermal behavior has been confirmed only in the case of undoped CaF_2, while at high Yb-doping levels the thermal conductivity stops depending on temperature [Popov, 2008], and at higher doping levels it might even decrease with cooling. The reason lies in the phenomenon of clusterization of Yb^{3+} ions in the hexameric structure, mentioned before. This leads to a decrease of mean-free-path of phonons that govern heat dissipation.

A possible solution to avoid this effect is to employ longer laser crystal with lower doping level.

4

Pumping system of multi-pass cryogenically cooled $Yb^{3+}:CaF_2$ amplifier

4.1 General description

As it has been underlined before, one of the advantages of $Yb^{3+}:CaF_2$ active medium is that it has ZPL that matches emission line of available laser diodes. ZPL of Yb^{3+}-doped CaF_2 is centered at ~976 nm, in the spectral region of powerful InGaAs laser diodes (LD), diode stacks and arrays. Therefore, Yb-doped calcium fluoride can effectively use pump radiation. Single-pass absorption coefficient accordingly to Beer's law:

$$\gamma(\lambda) = 1 - \exp\left(-\sigma_{abs}(\lambda) \cdot l \cdot N\right), \qquad \textbf{(4.1)}$$

where $\sigma_{abs}(\lambda)$ is the absorption cross-section spectrum, l is the crystal length, N is the concentration of Yb^{3+} ions in crystal.

In particular, the crystal implemented in our multi-pass amplifier has Yb^{3+} concentration of 2.8% and the length of 5 mm. Having these parameters, crystal absorbs ~70% of pump radiation in single pass under condition of good overlap of pump spectrum with absorption line of active medium, while in double-pass scheme crystal absorption equals to ~0.91, thus double-pass pumping is more desirable.

As a pump, powerful pulsed diode system by Lastronics has been employed (see fig. 4.1). This system consists of InGaAs laser diode array, which can produce up to 280 W of average power of pulsed radiation centered around 970-980 nm (depending on driving

current), emitted at repetition rate up to 100 Hz with a pulse duration of 2 ms and pulse energy $E = P/f_{rep} = 2.8$ J, where P is the average power, f_{rep} is the repetition rate.

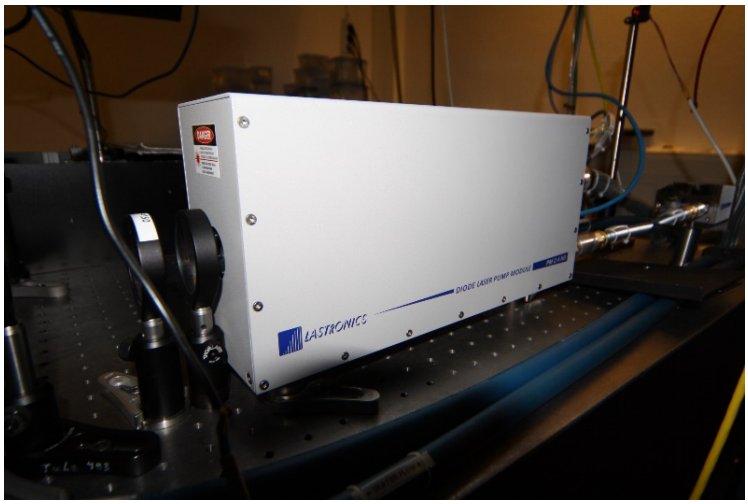

Fig. 4.1 Pump laser diode module by Lastronics

The radiation of array diode emitter has square cross-section. Next to the output window of the laser diode unit, a pair of positive lenses with focal distances of 400 and 150 mm focuses pumping beam and directs it through a round aperture to form its cross-section into round shape in order to improve an overlap of the seed and pump beams in the laser crystal. By tuning the distance between the two lenses, one can change effective focal distance of the pair according to the relation (4.2):

$$\frac{1}{f} = \frac{1}{f_1} + \frac{1}{f_2} - \frac{d}{f_1 f_2}, \qquad \textbf{(4.2)}$$

where f – is the effective focal distance of the lens system, f_1, f_2 are the focal distances of lenses 1 and 2, d is the distance between lenses 1 and 2.

The round aperture partially cuts the pump beam depending on the focal distance of the lens system. In the amplifier, focal distance was tuned in such a way, that the losses on the aperture were about 30% of the emitted power.

Curve presented in fig. 4.2 shows measured output power of pump diodes at different driving currents at 100 Hz repetition rate with and without the aperture.

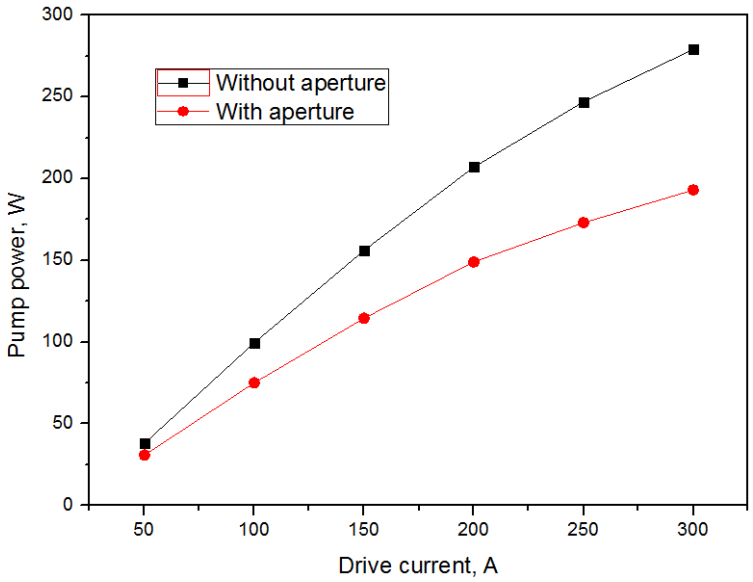

Fig. 4.2 P(I) curve of pump diode module with and without shaping aperture, 100 Hz repetition rate

As a result of the aperturing, the pump beam attains round cross-section with nearly uniform energy distribution.

Fig. 4.3 depicts the image of the cross-section of pump beam at the central plane of active medium, with following pumping parameters: driving current I_d = 100 A, repetition rate f_{rep} = 30 Hz. Figs. 4.4 and 4.5 represent cross-sections of pump beam shifted off the focal plane by 2 mm in both directions, which corresponds to the edges of active crystal, with the same parameters.

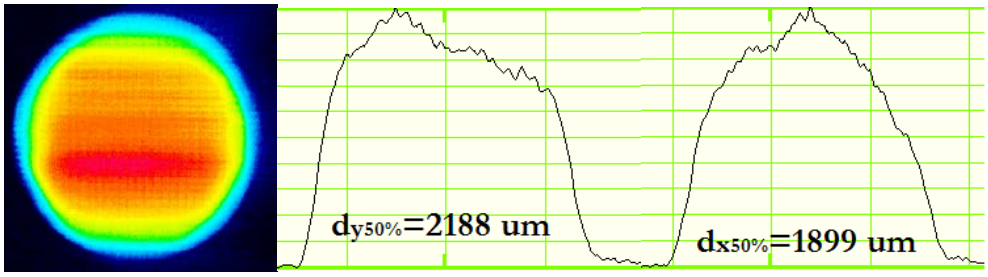

Fig. 4.3 Cross-section of pump beam at focal plane at 30 Hz repetition rate, 100A current supply, telescope reduction M = 2.5

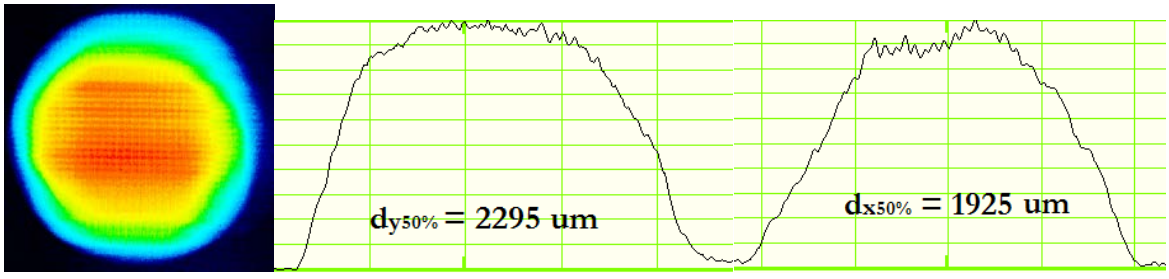

Fig. 4.4 Cross-section of pump beam at -2 mm off focal plane at 30 Hz repetition rate, 100A current supply, telescope reduction M = 2.5

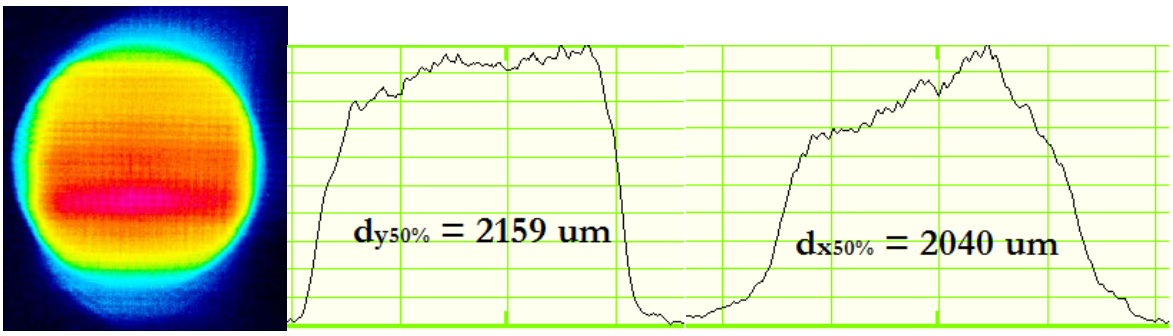

Fig. 4.5 Cross-section of pump beam at 2 mm off focal plane at 30 Hz repetition rate, 100A current supply, telescope reduction M = 2.5

Figs. 4.3-4.5 indicate that employed pump system allows obtaining a uniform round profile of population inversion, which is important in multi-pass scheme to mitigate conforming of seed beam profile to pump beam profile, which will be described in following chapters.

4.2 Various pump geometry schematics

As it has been underlined before, double-pass pumping system is advantageous and desirable in terms of efficient pump use. However, implementation of double-pass scheme poses challenge of isolation of pump LD from back propagating pump radiation that can damage it. To realize a double-pass scheme, several approaches can be used. One scheme has been employed in regenerative preamplifier (RA) [Pugzlys, 2009], that serves as a seed source for considered multi-pass power amplifier. In RA setup, spatial shift is introduced by a retro-reflector to the pump beam after the first pass, so that it propagates second time through the active medium at an angle to the first pass and thus along the different path and eventually is blocked by a beam dump (see fig. 4.6). This approach is feasible only when pump beam diameter is relatively small and expands slowly after the first pass. Otherwise, too big pump beam diameter will require large aperture mirrors to shift and reflect it and will lead to bigger angles between forward and backward passes, which will lead to a crop of pump beam by the aperture of the crystal or its vacuum chamber.

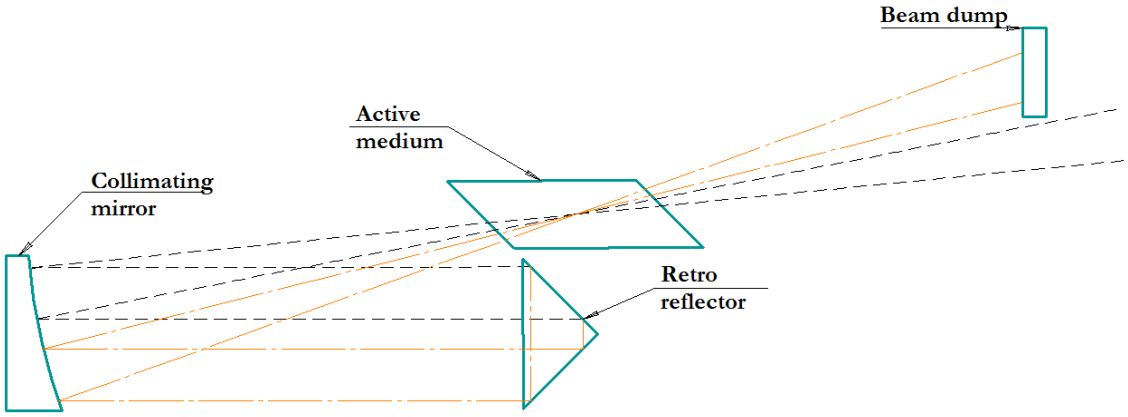

Fig. 4.6 Double-pass scheme with spatial beam shifting

This scheme is advantageous, since allows blocking of residual radiation after the second pass. In the case when pump beam strongly diverges after the first pass and has a large diameter on the collimating mirror, the scheme sketched in fig. 4.7 can be used. In this scheme, no spatial shift of the beam is introduced and the pump beam propagates along the same path forward and backward. Protection of the diode is performed in this case by means of polarization control. Linearly p-polarized pump radiation, partially transmitted through active medium and diverging, passes quarter-wave plate (QWP). Its polarization transforms to circular. After reflection at the concave mirror M1, to active medium, pump radiation passes QWP for the second time and acquires additional quarter-wave path difference, thus transforms its polarization to linear, orthogonal to that of the forward-propagating beam.

Finally, the beam propagating backwards is reflected by a thin film polarizer (TFP) and thus prevented from entering pump diodes. The drawback of this approach is that the backward propagating pump radiation experiences losses on the Brewster-angled edges of the laser crystal.

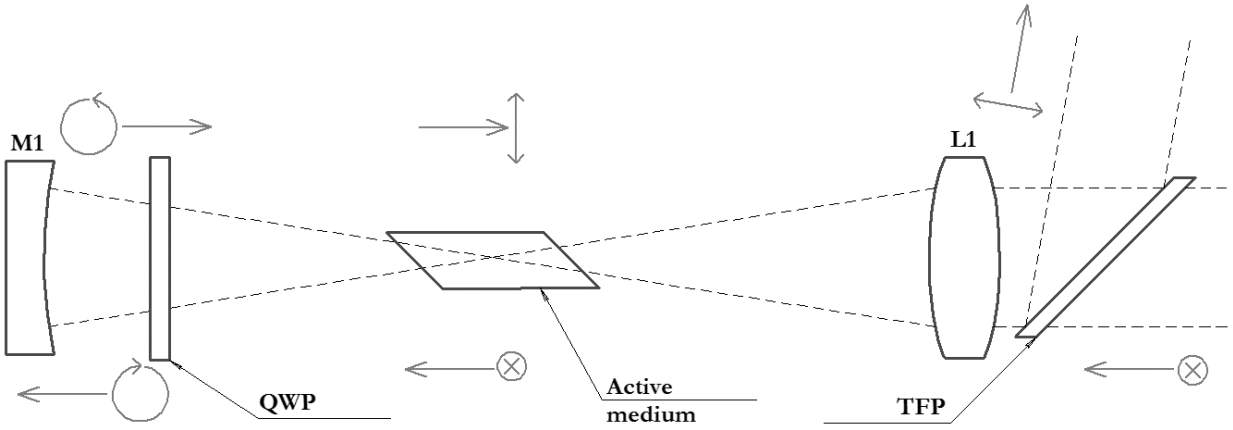

Fig. 4.7 Double-pass pumping schematics.

The implementation of double-pass scheme requires large aperture custom-made QWPs, which during the work were not available in the laboratory. In this Master thesis a single-pass longitudinal pumping geometry shown in the fig. 4.8 was employed.

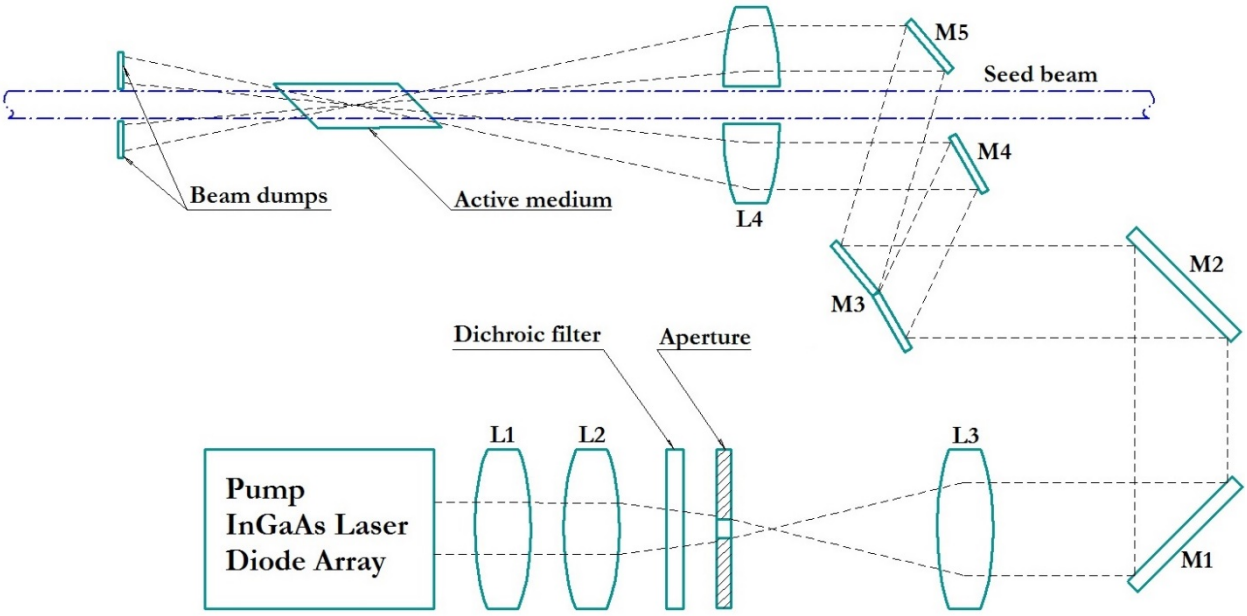

Fig. 4.8 Pumping geometry in a single-pass pumping scheme of multi-pass amplifier

Often, in multi-pass systems pump radiation is delivered to the crystal through the dichroic mirror. The optical damage threshold of dichroic optics is around 5 J/cm^2, which is half of Yb:CaF_2 threshold. For this reason, dichroic mirrors would not withstand intensities

existent in our multi-pass system. Therefore, we had to develop more complicated pumping schematics. In our system, pump beam of the Lastronics laser diode is shaped by the focusing system consisting of lenses L1 and L2 and the aperture. Dichroic filter is also provided in order to protect laser diode array from back-scattered seed radiation. Afterwards, pump beam is collimated by a lens L3 with f = 500 mm focal length. The collimated beam is then divided to two by large aperture square-shape metal mirrors M3 and M4 and is focused by two halves of spherical lens L4 into active medium from two directions, equally angled to the seed beam path. Such arrangement ensures that seeded beam can freely propagate unclipped by the elements of the pump system. After propagation through the active medium, pump beam is blocked by beam dumps (~30% of incident beam energy).

4.3 Thermal deviations of pump spectrum

When laser diodes are driven at high currents, the drift of the emission wavelength occurs because the change of LD temperature takes place. Usually, the LD manufacturers solve this problem by using Bragg gratings in LD system, which stabilize the wavelength and prevent it from the temperature and current dependent drifts. In the Lastronics pump module, no Bragg gratings provided due to technological complications, thus the current and temperature ranges should be carefully selected in order to match the absorption line of active medium. Fig. 4.9 represents the dependence of the normalized diode emission spectrum on the driving current at 100 Hz repetition rate. With increase of the current, diode emission line red-shifts, and emission peak drifts from ~969 nm at 50 A to ~986 nm at 300 A. Fig 4.10 depicts the selected spectral lines of the diodes at different currents at 100 Hz repetition rate in comparison to absorption spectrum of the active medium, which peaks at 976 nm.

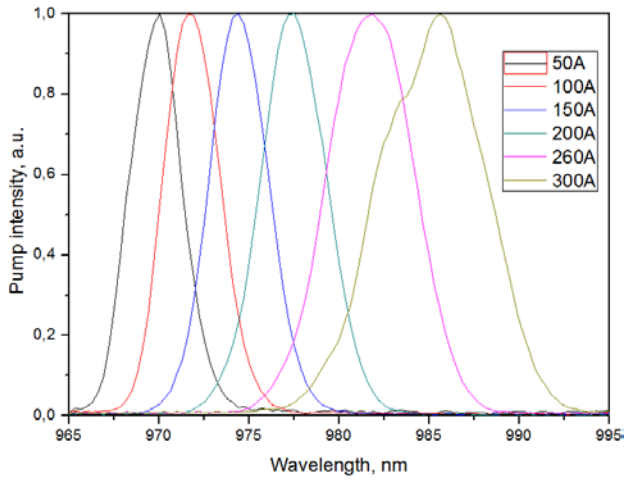

Fig. 4.9 Dependence of pump emission spectrum on driving current, 100 Hz

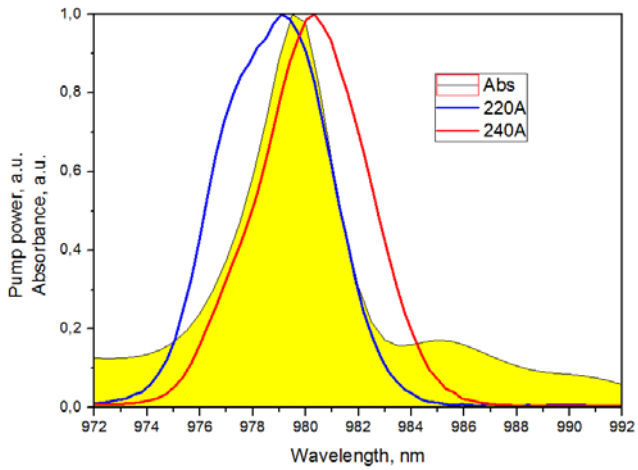

Fig. 4.10 Overlap of the pump spectrum with the absorption spectrum of the active medium at different driving currents, 100 Hz

It can be seen from fig. 4.10 that the emission line at 220 A matches the absorption line optimally, while already at 240 A the spectra start losing an overlap, and pump emission line red-shifts. Thus, at 100 Hz repetition rate optimal driving current for the pump module is 220 A, which corresponds to the output pump power of 158 W. According to specifications the pump module can produce 193 W power at 300 A driving current (see fig. 4.2). The performance of pump module at 100 Hz repetition rate is restricted. When lower repetition rate is used, the thermal load of the diode stacks decreases, which leads to a less distinctive spectrum drift, as depicted in fig. 4.11.

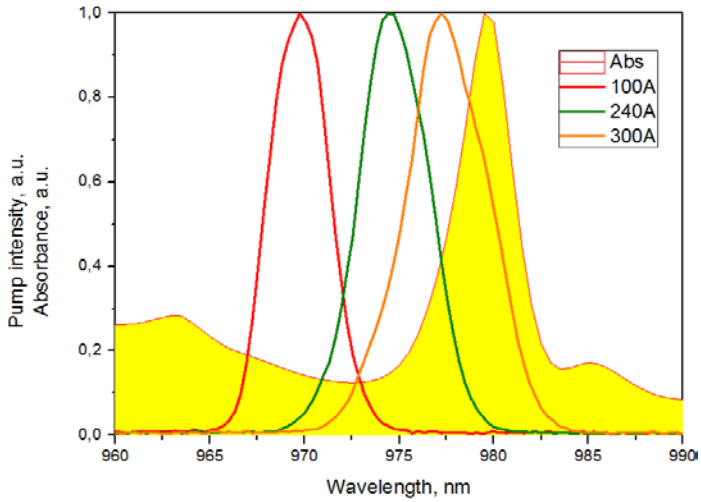

Fig. 4.11 Overlap of pump spectrum with active medium absorption spectrum at different driving currents, 50 Hz

Having described arrangement of the pump module and characterized its performance, we will in following consider schematics of multi-pass amplification scheme.

5

Multi-pass cryogenically cooled amplifier system

5.1 Multi-pass geometric arrangement

In the developed system multi-pass amplifier serves as a second stage amplifier for the output of cryogenically cooled Yb:CaF_2 regenerative amplifier, described in details in [Pugzlys, 2009]. The RA stage is seeded by solid-state Yb:KGW master oscillator (MO), which emits 6.5 nJ pulses at 75 MHz repetition rate stretched to ~500 ps duration. The RA is pumped by InGaAs diode stacks operating in cw mode and amplifies 500 ps pulses with broad spectrum of ~10-12 nm, which corresponds to ~200 fs transform limited pulse duration, up to 10 mJ output pulse energy. When not seeded, the RA operates in Q-switched regime (self-oscillating) and generates 10 ns pulses.

Because of the tight focusing of the amplified pulse in the RA, the output energy is limited by the optical damage threshold of the active medium or the Pokkels cell crystal and by extensive accumulation of B-integral (5.1).

Optical damage threshold of Yb:CaF_2 crystal is presented in fig. 5.1 and scales with square root of pulse duration [Stuart, 1995].

$$B(r) = \frac{2\pi}{\lambda}\int_0^l n_2 I(r,z)\,dz\,, \qquad \textbf{(5.1)}$$

where z is the coordinate along propagation direction, r is the radial coordinate of the beam, n_2 is the nonlinear refractive index, l is the length of the crystal, $I(r,z)$ is the radiation intensity along propagation axis and transversal radius-vector. In order to achieve higher pulse energies, a subsequent to RA amplification stage is necessary.

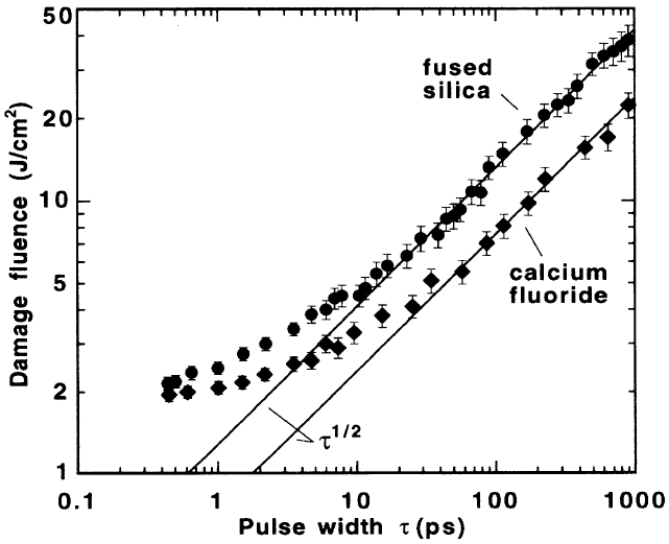

Fig. 5.1 Dependence of the damage threshold of CaF_2 and fused silica at 1053 nm on the pulse duration [Stuart, 1995]

At 500 ps pulse duration threshold fluence equals accordingly to fig. 5.1 ~18 J/cm^2. Therefore, target 100 mJ pulses can be achieved with the beam diameter in active medium not less than 2.2 mm.

Scaling of the beam diameter is realized with refractive telescope is placed in between RA and MP amplifier stages.

The geometry of the multi-pass amplifier is based on 4f imaging system, as is depicted in fig. 5.2.

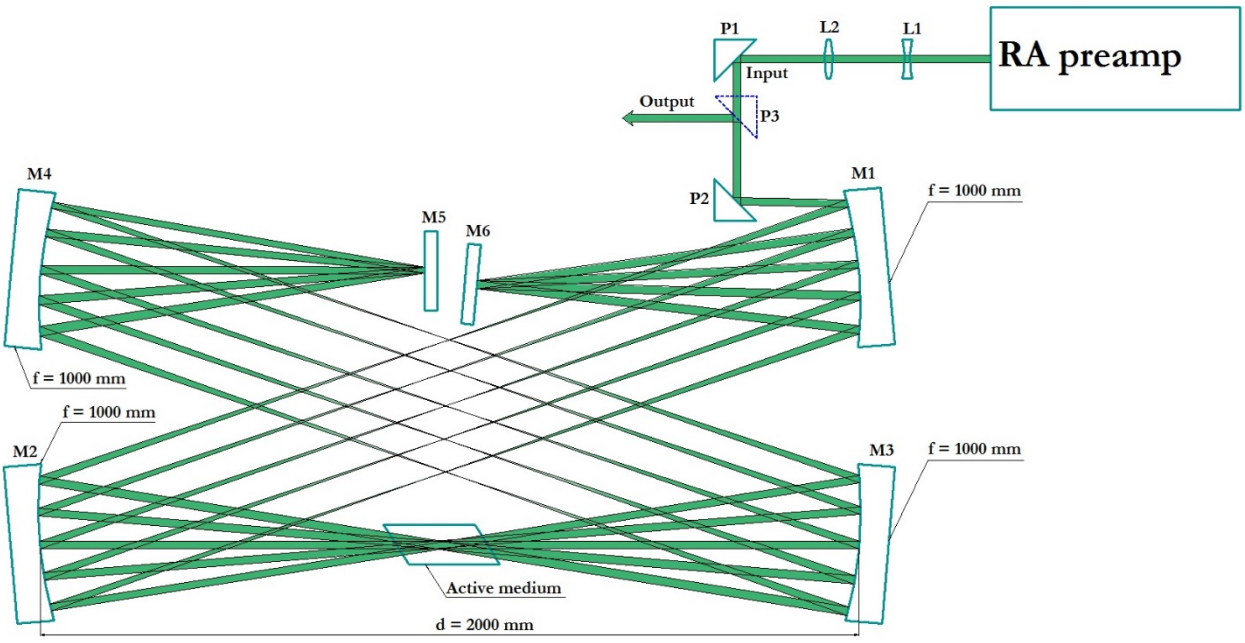

Fig. 5.2 Geometric arrangement of the multi-pass amplifier

Seed beam from the RA is collimated and directed into MP with prisms P1, P2 at the mirror M1 with f = 1000 mm. Mirror M1 reflects input beam to the mirror M2, which has the same curvature as M1. Mirror M2 collimates the beam and feeds it into an active medium. Then, M3 and M4 with the focal distances of 1000 mm each make an f-2f-f imaging of the middle plane of the active medium to a flat mirror M5, which rebounds the beam to the next pass.

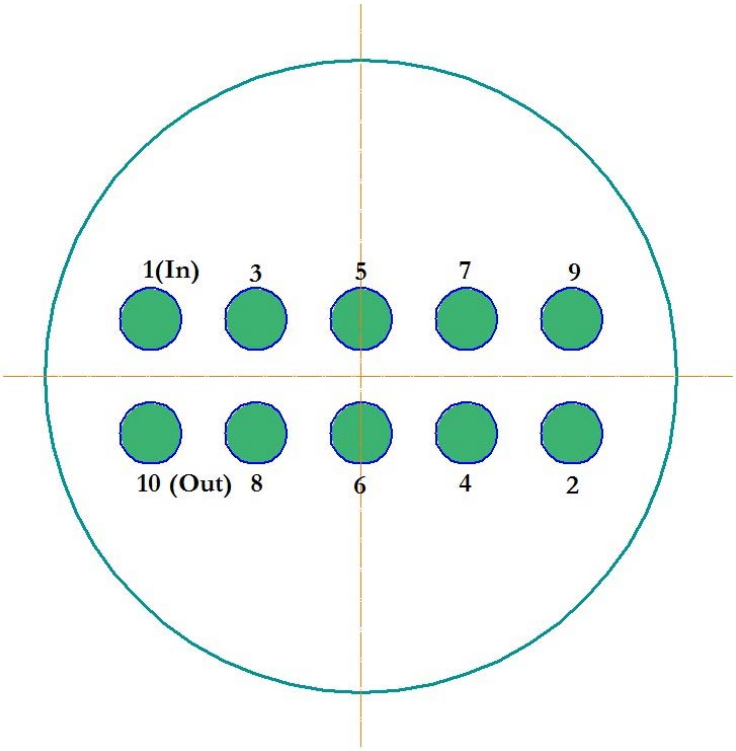

Fig. 5.3 Positions of different passes on M1 mirror

The amplified beam is outcoupled along the same path as an input, but shifted downwards. The number of passes can be set by adjusting the angle of the flat mirror M6. We used 10 passes setup during the measurements and characterization of the MP amplifier arrangement, as depicted in fig. 5.3.

The active medium of MP amplifier was cryogenically cooled, since operation at low temperatures leads to significantly improved performance, as has been described in the chapter 3.4. As a cryorefrigerator, single-stage pulsed cryocooler PT90 by Cryomech has been employed (fig. 5.4 a), which is capable of maintaining temperature of 80 K at 90 W heat load.

The crystal was fixed with indium foil on the interface of copper holder (fig. 5.4 b) and was protected at the edges from pump and amplified radiation by sharp-edge mirrors, in order to prevent melting of indium foil during operation.

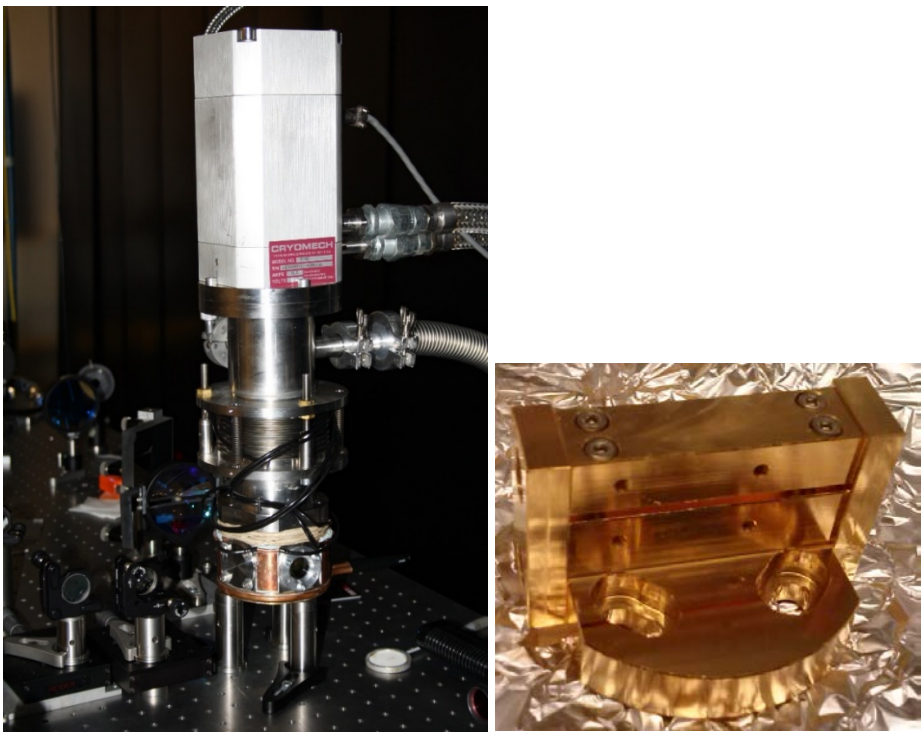

a). b).

Fig. 5.4 a). Vacuum chamber with installed crystal holder attached to cryorefrigerator, **b).** Crystal holder

The holder of the crystal was attached to the cold finger and inserted into vacuum chamber shown in fig. 5.4 a. The Yb:CaF_2 crystal with Yb^{3+} doping level of 2.8% was 5 mm long and 3 mm high.

The concentration of active ions has important influence on the performance of the amplifier. On the one hand, higher doping concentrations leads to shorter pump absorption length, thus more effective use of the pump radiation, higher population inversion density, and, consequently, allows higher gain and higher slope efficiency. On the other hand, high dopant concentration significantly worsens thermal conductivity, which eventually leads to higher thermal gradients within the gain medium and thus severe thermal lensing and depolarization losses. Therefore, a trade-off between the high gain and thermal effects should be sought for. Crystal with 2% doping was also tested, but exhibited worse performance.

5.2 Small-signal gain

In order to characterize the performance of the above described MP amplifier, small-signal gain measurements have been conducted. This allows evaluation of round-passes and seed energy needed to reach the required level of the output energy as well as estimation of energy stored in the active medium.

Small-signal gain measurements have been conducted for pump driving currents in the full range from 0 to 300 A. The pump beam has been cropped by the aperture, in order to achieve a uniform round distribution of the population inversion in the gain medium, as described in chapter 4.1. Pump repetition rate was set to 100 Hz during the measurement. The results of the measurements are presented in fig. 5.5.

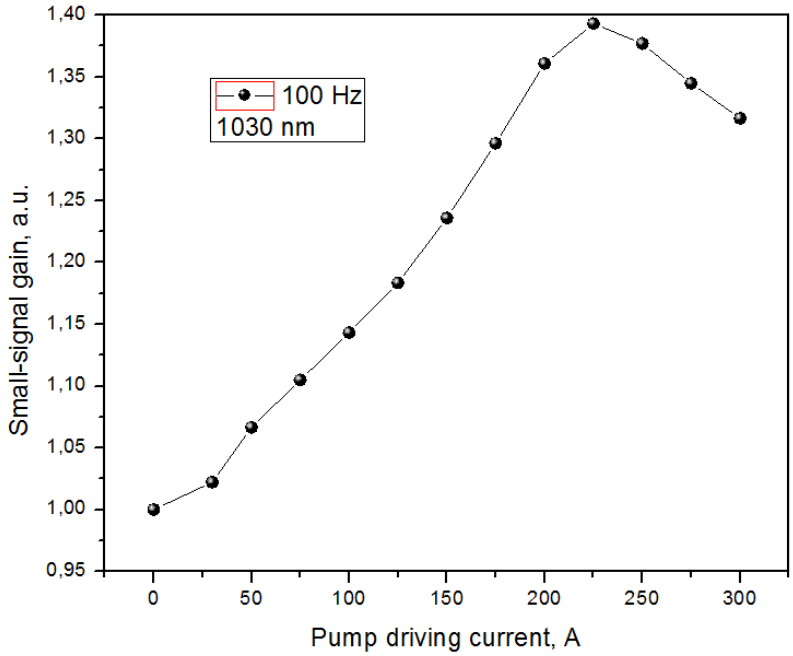

Fig. 5.5 Dependence of the small-signal on the pump driving current (~30% cropped pump beam, @ 100 Hz, 2 ms pump pulse duration)

Small-signal gain increases nearly linearly with driving current and reaches its maximum of 1.393 at 225 A, which corresponds to 142 W of pump power. Beyond this point, small-signal gain suffers gradual decrease, which is linked to the drift of pump spectrum, discussed in chapter 4.3. As it follows from fig. 4.10, the optimal pump driving current at 100 Hz frequency allowing the best overlap of the diode emission line and gain medium absorption line lies between 220 A and 240 A. This value is below the limit of the diode capability, which prevents achieving best performance of the pumping system. All the

available pump power can be used at lower repetition rate of the pump module. We therefore conducted preliminary characterization at the lower repetition rate of 50 Hz, which allowed reaching best small-signal gain parameters at a driving current of 300 A (see fig. 4.11).

5.3 Output pulse energy

Characterization of the MP amplifier performance in terms of extractable output energy has been conducted with 10 ns seed pulses in the case of 10 passes through the active medium.

Fig. 5.6 represents the dependence of the output energy on absorbed pump energy. After 10 passes 1.2 mJ seed pulses are amplified to 26 mJ with 1.67 J absorbed energy. Output pulse energy scales exponentially with absorbed pump energy which indicates an absence of pump and gain saturation.

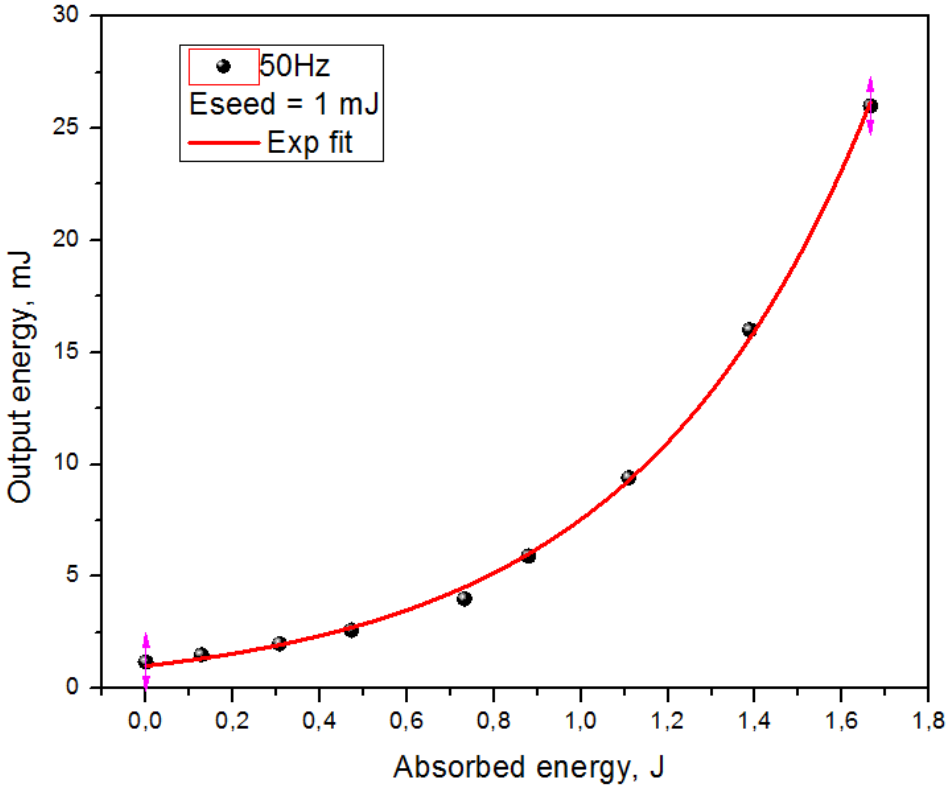

Fig. 5.6 Dependence of the output pulse energy on absorbed pump energy at 50 Hz repetition rate for 500 ps pulses after 10 passes in the gain medium

As it is shown in fig. 5.7, at 3 mJ seed energy the output energy of MP amplifier was 52 mJ. The output pulse energy scales linearly with seed energy, which also indicates that amplifier operates far from saturation. Consequently, further increase of seed energy is potentially advantageous, however beam narrowing escalates the risk of optical damage of the gain medium. In order to increase the seed pulse energy and reach higher output energy level, we need first to be able to control the beam diameter and maintain its value.

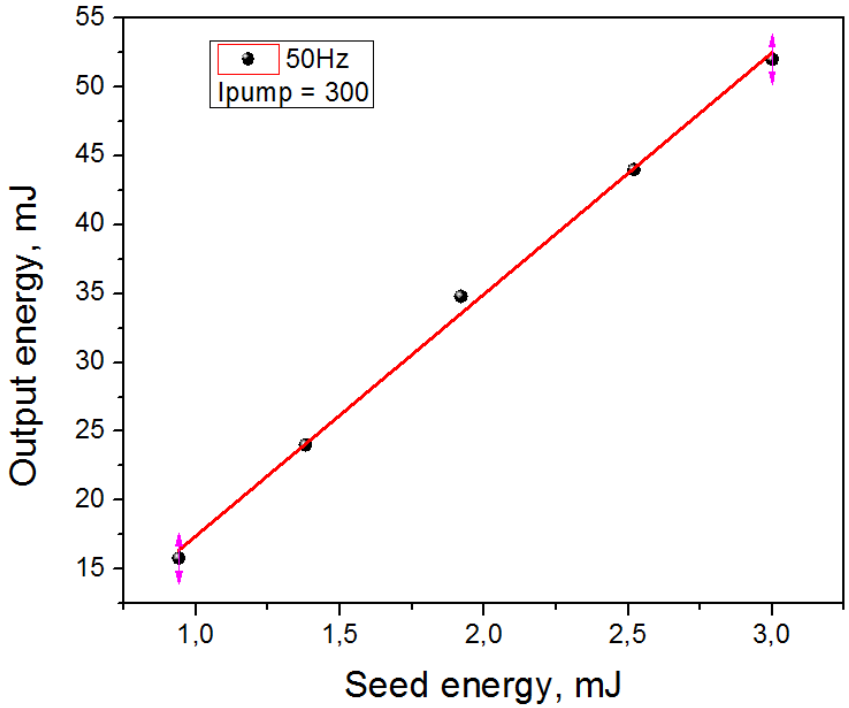

Fig. 5.7 Dependence of output pulse energy on seed pulse energy at 50 Hz repetition rate under 300 A pump driving current for 500 ps pulses after 10 passes in the gain medium

5.4 Output beam profile

One of the major problems that arise during development of MP amplifiers is beam distortions, which occur due to the thermal lensing, self-phase modulation (SPM) in gain medium or due to spatial and spectral gain narrowing and shaping.

5.4.1 Self-phase modulation

Self-phase modulation (SPM) occurs when the radiation with high intensity propagates through the active medium. The pulse accumulates nonlinear phase-shift, described by B-integral (5.1), which leads to self-focusing of the beam and may eventually cause optical damage of the gain medium. An approach to diminish SPM consists in keeping radiation intensity in gain medium sufficiently low, so that cumulative B-integral does not exceed critical value of π [Siegman, 1986]. This can be achieved by scaling up the beam diameter or by stronger stretching of seed pulses. SPM problem is more pronounced in case of RA due to high number of passes in the gain medium. In the case of MP amplifier, the number of passes is substantially lower, and given that the amplified beam has input diameter of d~2.6 mm, SPM effect does not contribute much into the output beam distortion.

5.4.1 Thermal lensing

On the contrary, thermal effects that occur in the amplifier gain medium, affect beam profile considerably. First, CaF_2 crystal attains negative thermal lens due to the thermal gradients that inevitably occur when the crystal is pumped. Additional negative lens causes alteration of optical arrangement of MP scheme and leads to breach of 4*f* imaging condition. Dioptric power of the thermal lens under assumption of evenly distributed heat load writes as follows [Paschotta, 2008]:

$$f^{-1} = \frac{dn/dT}{2\kappa A} P_{heat}, \qquad \textbf{(5.2)}$$

where κ is the thermal conductivity, A is the pumped area, P_{heat} is the dissipated pump power.

Alternation of the focal distance introduced by the thermal lens can be compensated by adjusting the position of mirror M4 to a certain pump condition to maintain imaging of the beam profile in the middle of the crystal. The compensation is different for different pump powers; therefore, diminishing of the thermal lens in crystal is desired.

Thermal gradients causing thermal lensing effects, can be reduced in several ways. First, by applying cryogenic cooling to the crystal that leads to substantial increase of thermal conductivity, which aids better heat dissipation and consequently lower thermal gradients in the active medium. The thermal conductivity is severely affected by doping concentration. With increase of doping level, thermal conductivity drops rapidly. On the other hand, low doping levels lead to low pump efficiency and gain. Therefore, appropriate trade-off between the gain and the thermal conductivity should be found. In our system, 2.8% doped Yb^{3+}:CaF_2 cryogenically cooled crystal was performing the best.

5.4.1 Spatial gain narrowing

Spatial gain narrowing originates from the fact that spatial pump energy distribution is not uniform. Mathematically, amplification of the seed beam corresponds to multiplication of its spatial profile and spatial gain profile, which is described as follows:

$$I_{out}(x,y) = I_{in}(x,y)\left[G_{RT}(x,y)\right]^{N}, \quad \textbf{(5.3)}$$

where N is the number of passes through the active medium. Expression (5.5) only gives a qualitative description of the phenomenon, since in reality, pulse in a MP amplifier makes each pass along the slightly different direction, and thus G_{RT} profile for each pass slightly differs. The gain can be described in a small-signal gain approximation, which can be assumed in our case, as has been confirmed by output energy measurements:

$$G_0(x,y,z,\lambda) = \exp\left(\sigma_{em}(\lambda)\Delta N(x,y)z\right) \quad \textbf{(5.4)}$$

where $\sigma_{em}(\lambda)$ is the emission cross-section, $\Delta N(x,y)$ is the population inversion, z is the direction along the laser crystal.

Spatial distribution of the population inversion is proportional to the pump flux distribution, which always has a roll-off at the edge. As a result, edges of the beam are less amplified than its central part in each pass. After several passes this may lead to substantial decrease of beam diameter and thus to increase of radiation intensity in the gain medium, which eventually may cause optical damage of the crystal.

Another aspect of the spatial narrowing is connected with nonhomogeneous gain profile, which occur when uniformity of the pump beam is not achieved. In this case, the gain medium can act as a set of micro-lenses and severely distort the output beam profile. In extreme cases, it may lead to filamentation of the beam. In order to eliminate this, high evenness of spatial energy distribution of the pump beam should be achieved. Besides, spatial gain narrowing effect can reshape output beam if pump beam profile does not match amplified beam profile. For example, we have initially attempted to use uncropped pump

beam in order to use pump energy more efficiently, but it has led to square output beam profile, depicted in fig. 5.8b.

Evidently, pump beam can efficiently re-shape the output beam profile, thus it has to be shaped in an appropriate manner. In the case, presented in fig. 5.8, driving current of 300 A at 50 Hz repetition rate has been applied, while 1 mJ 10 ns seed pulses in 10 round trips, were amplified to 20 mJ output pulse energy. This corresponds to the measured small-signal gain value of ~1.35.

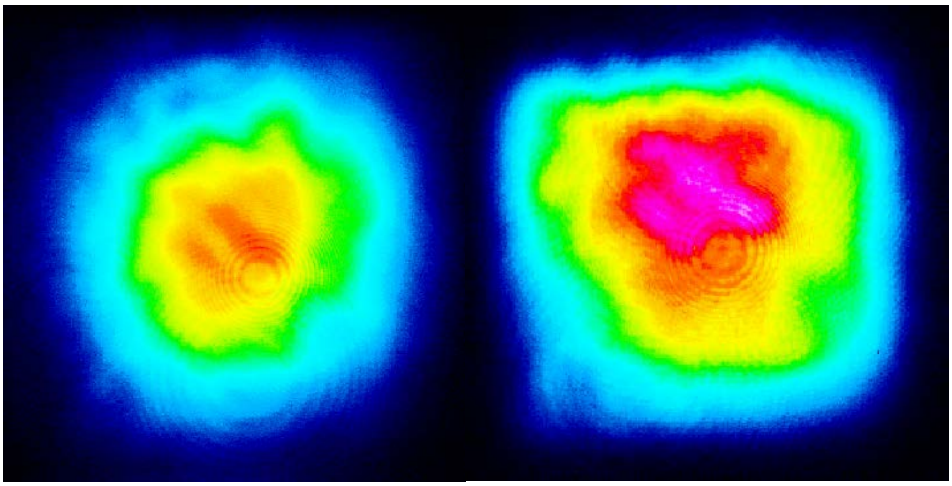

a). b).

Fig. 5.8 a). Input beam profile **b).** Output beam profile with square pump beam

When we implemented round aperture, output beam profile depicted in fig. 5.9b has been achieved:

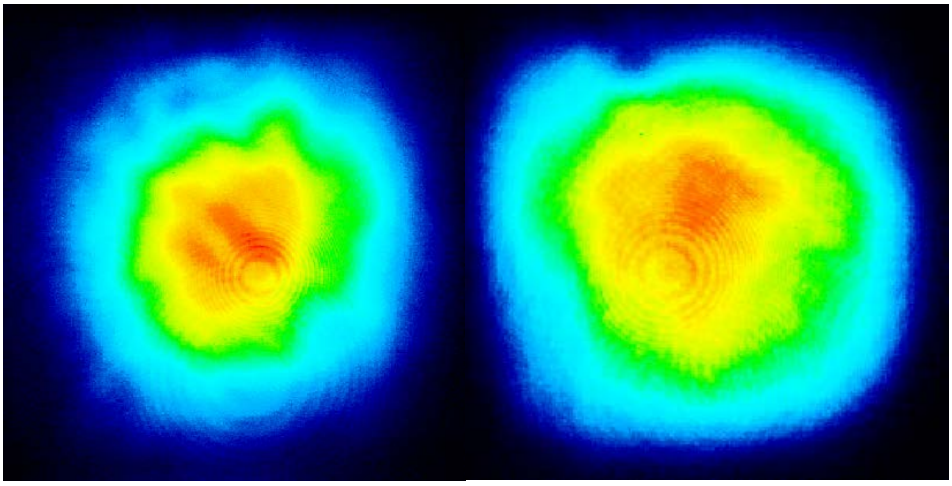

a). b).

Fig. 5.9 a). Input beam profile **b).** Output beam profile with round pump beam

In the latter case, the amplified beam does not display severe deviations from the desired round shape. No filamentation or rippling was observed.

Therefore, shaping of the pump beam with round aperture has been considered advantageous and has been implemented during all the conducted measurements. On the other hand, it sets certain trade-off between the output beam quality and pump power, which decreases by approximately 30%.

According to the data presented in fig. 5.1, at 100 mJ 500 ps pulse the desirable pump diameter equals 2.2 mm. In our setup, the beam diameter collapsed after 10 passes down to 1.6 mm. Consequently, in order to reach target 100 mJ energy, the beam diameter needs to be expanded.

5.5 Beam diameter control

The solution that allowed to overcome the problem of beam narrowing required rearrangement of the MP schematics. The idea is to expand the beam diameter after several passes and to reinsert the expanded beam back into MP amplifier for further amplification. The scheme of the rearranged MP amplifier is presented in fig. 5.10.

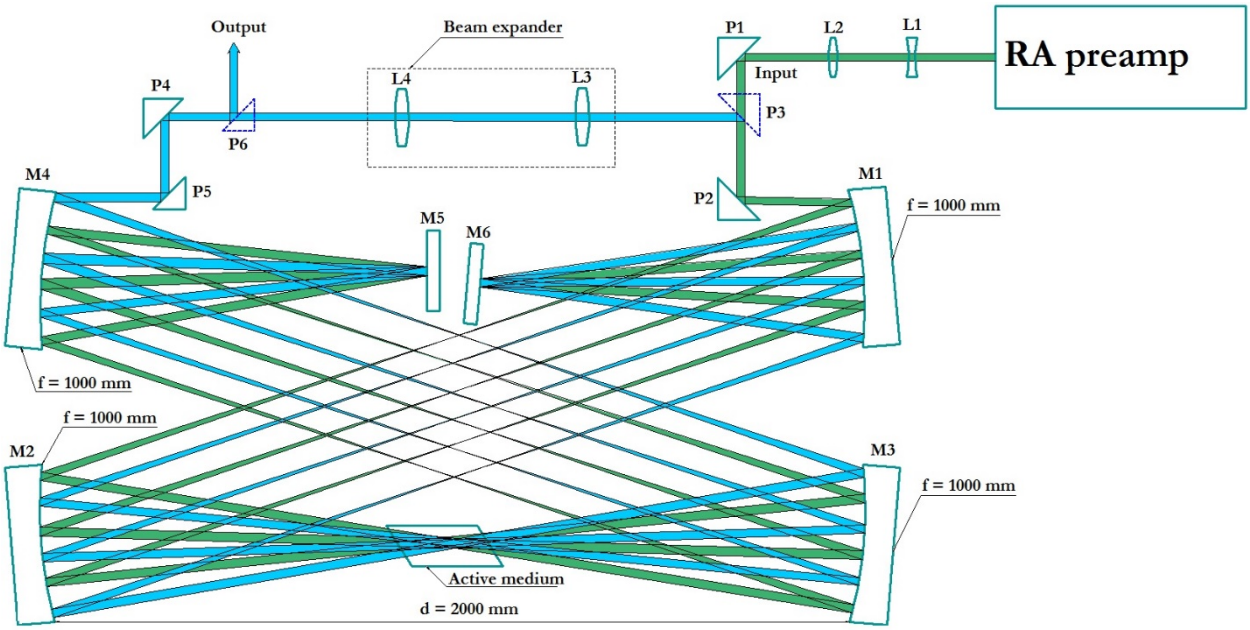

Fig. 5.10 Multi-pass geometry with the ability to control beam diameter

In this setup, input beam is directed into MP amplifier by prism P2 and makes 6 passes, depicted in green. After the sixth pass beam narrowing becomes pronounced and beam is picked up from MP by P3 prism. Then, the beam is magnified by lens telescope to have diameter of 2.6 mm and reinserted back into MP amplifier.

After the expansion, pulses make another six passes along different path, represented in blue, such as depicted in fig. 5.11.

In this geometrical arrangement, pulse makes 12 round passes which is advantageous in terms of overall gain of the system.

With this approach, we managed to keep the beam diameter sufficiently large and eventually obtained desirable energy level of 100 mJ at 50 Hz repetition rate at 300 A diode driving current. The input pulse energy was ~7 mJ seed pule energy. Beam profile at 100 mJ output is presented in fig. 5.12 in comparison to the input beam profile, which confirms an absence of severe artifacts and shape distortion in the MP amplifier.

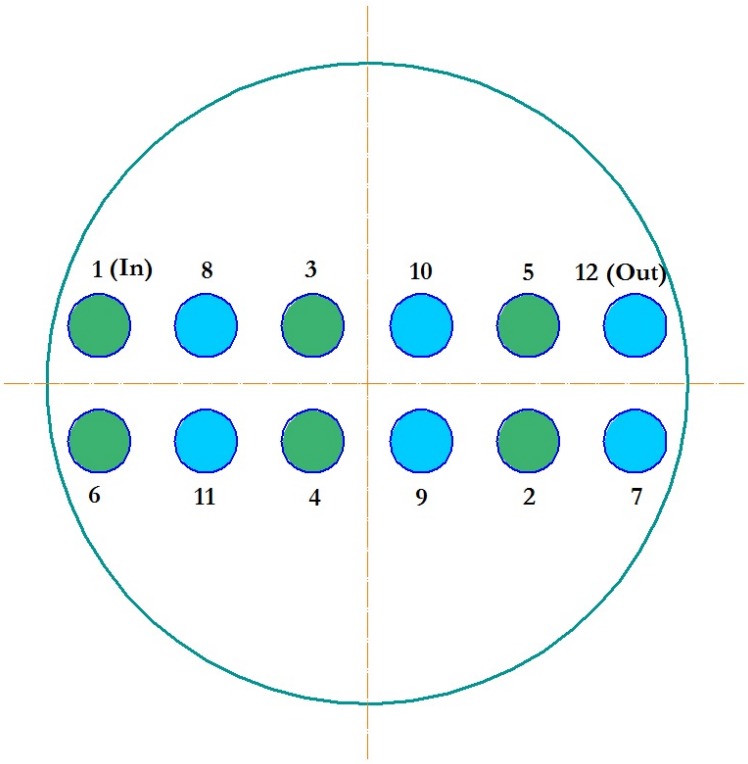

Fig. 5.11 Position of passes on MP mirror with ability to control beam diameter

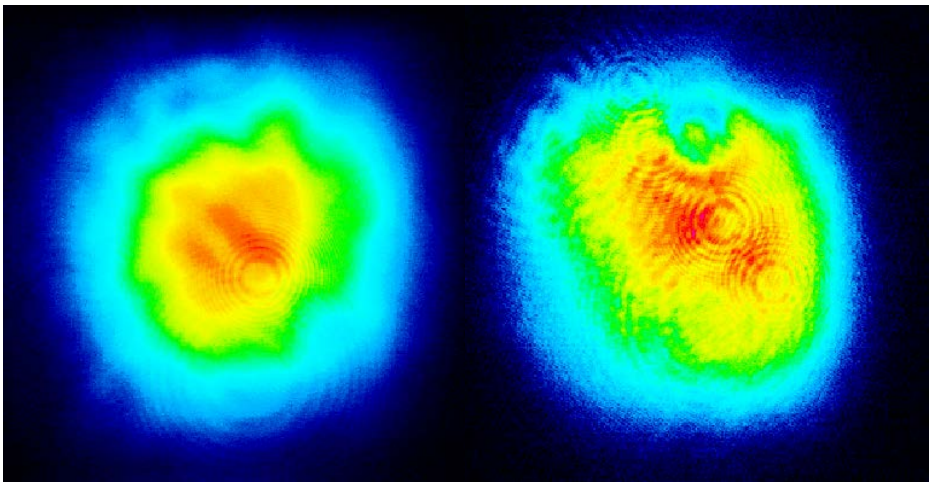

a). b).

Fig. 5.12 a). Input beam profile b). Output beam profile

The diameter of amplified beam in the active medium due to use of expander amounts to ~2.2 mm at 12^{th} pass, which is safe for CaF_2 crystal:

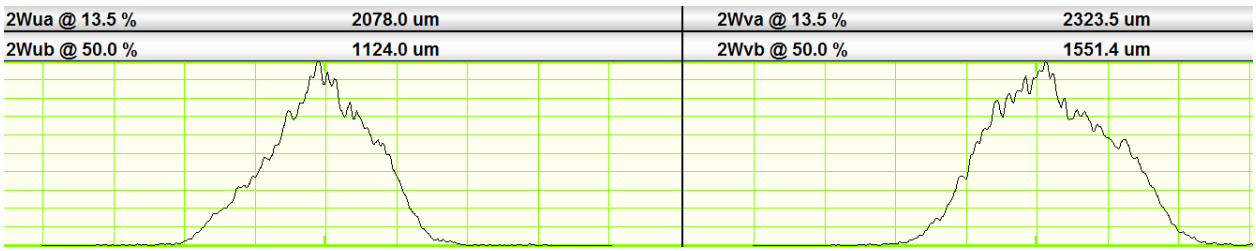

a). b).

Fig. 5.13 Output beam profile cross-section along a). x and b). y axis

Slope of the output energy exhibits tendency to saturation, as can be seen from fig. 5.14, and confirms achievement of 100 mJ output pulse energy.

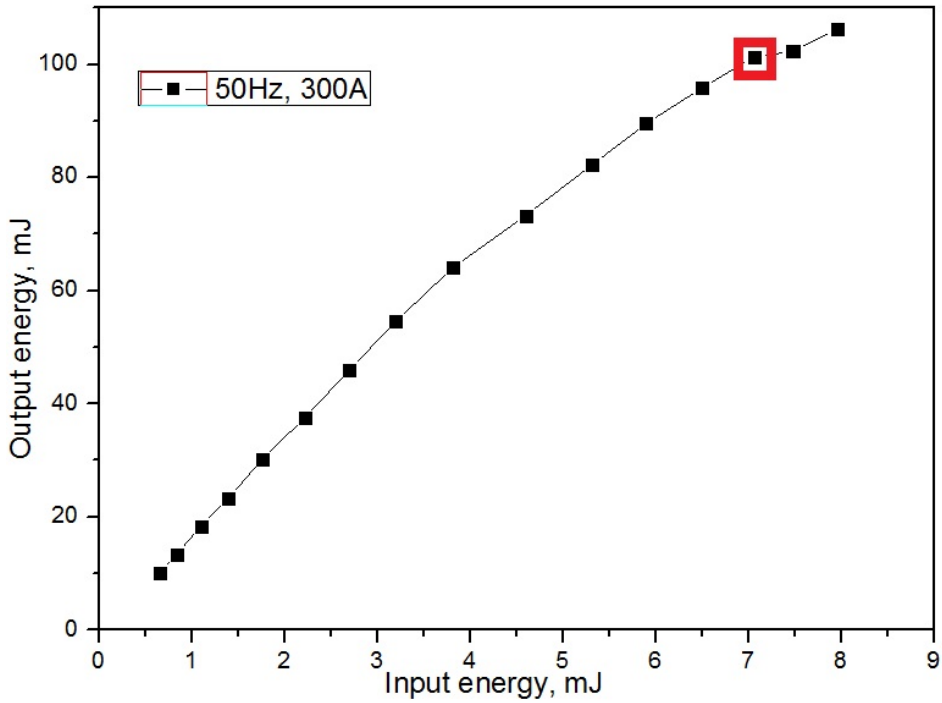

Fig. 5.14 Output pulse energy, 500 ps broadband pulses

Recorded output spectrum of 100 mJ pulses is shown in fig. 5.15. It has ~10 nm spectral bandwidth at FWHM and is slightly narrowed at FWHM level as compared to the input spectrum. On the edges of the spectrum, broadening is observed, which attributes to the SPM effect in the air. In order to eliminate this broadening, beam waists needs to be encapsulated into the vacuum chamber.

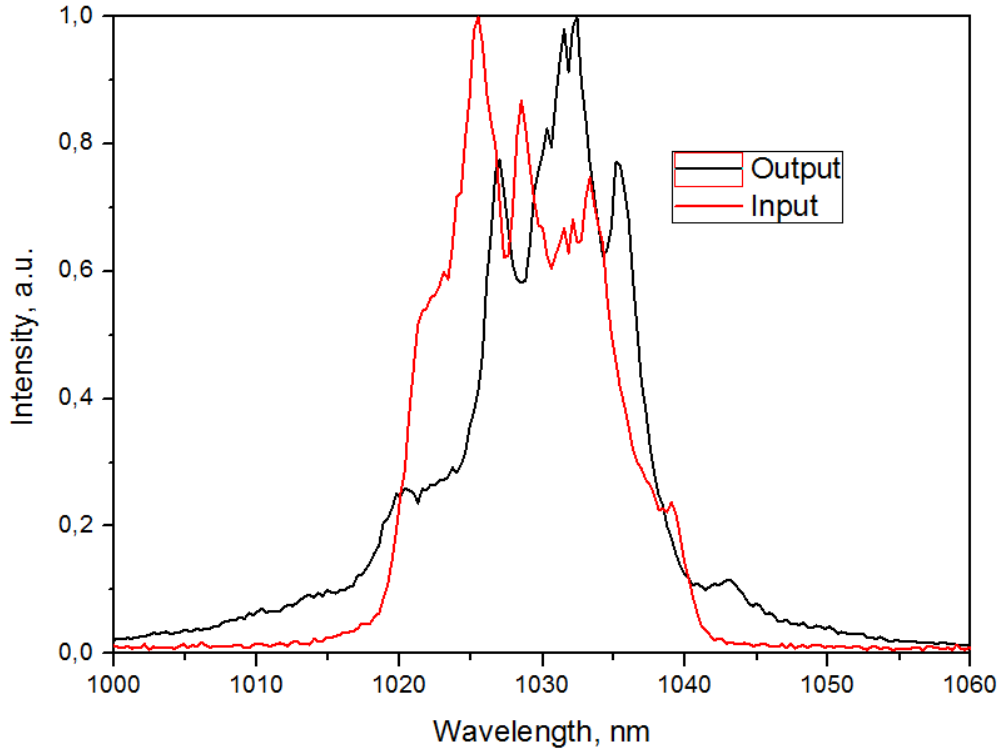

Fig. 5.14 Output and input spectra, 100 mJ pulse

6

Numerical modelling of the bonded crystal

6.1 Theoretical background

The results reported in the previous chapter confirm successful amplification of 500 ps seed pulses up to 100 mJ energy level. However, the desirable repetition rate has of 100 Hz not been achieved. One of the approaches to increase the average power of the MP amplifier while maintaining the pulse energy constant is to improve heat extraction from the active medium.

In the developed cryogenically cooled system, the laser crystal is slab-shaped and end-pumped. The cooling is realized from the top and the bottom sides, where the crystal has a contact with the copper holder. Heat extraction from the crystal might be more efficient if the deposited heat could also dissipate through the faces of the laser crystal, where the temperature reaches its highest values. In order to realize heat sinks on the faces of the laser crystal, we offered to attach the cylindrical disks of blank, undoped CaF_2 to the active, Yb-doped CaF_2 by means of thermal bonding. Then, this structure is attached to the cryogenically cooled ring-shaped copper heat-sink with an indium foil. The cross-section of this structure is depicted in fig. 6.1.

In order to study thermal behavior of this arrangement, we performed numerical modelling in Comsol Multiphysics software, which uses finite element methods [Chaskalovic, 2008] to solve differential equations that describe various physical processes. We used steady-state analysis presets of general heat transfer preset in the Heat Transfer Module of Comsol for our simulations.

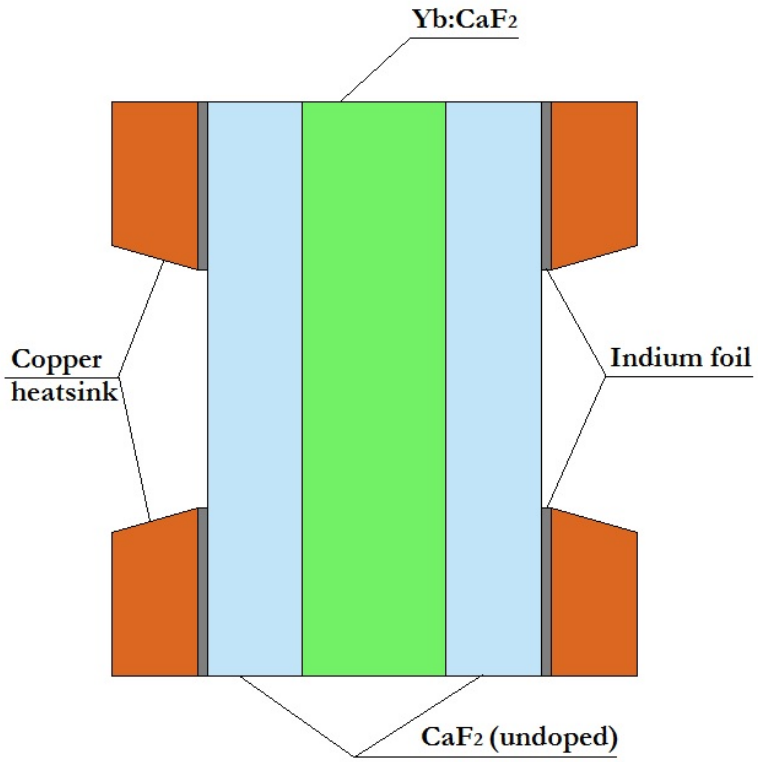

Fig. 6.1 Sketch of the cross-section of modelled laser crystal arrangement

Spatial and temporal distribution of thermal gradients in the medium is governed by heat equation [Chenais, n.d.]:

$$\rho C_p \frac{\partial T(x,y,z,t)}{\partial t} - K_c \nabla^2 T = Q_{th}(x,y,z), \qquad \textbf{(6.1)}$$

where T is the temperature in K, ρ is the density of the material in kg*m^3, C_p is the specific heat of the material in J/(kg*K), K_c is the thermal conductivity of the material in W/(m*K), Q_{th} is the thermal load per unit volume in W/m^3.

We assume that the heat source in the crystal is constant and has 200 W power, specified by the pump module we use in our system, i.e. we consider steady state of thermal distribution in the laser crystal. Therefore, we dismiss the first term in (6.1). Density and specific heat therefore do not influence the calculation.

Initial temperature for the calculations is 100 K – approximate cryogenic temperature, at which our system operates. Copper, indium, blank and doped CaF_2 have following thermal conductivities at this temperature:

Table 2 Thermal conductivities of materials at 100 K

Material	Thermal conductivity, W/m*K
Copper	483 [Davis, 2001]
Indium	82 [NBS]
CaF_2	50 [Corning, 2003]
$Yb^{3+}:CaF_2$	5 [Siegman, 2009]

The thermal load Q_{th} originates from the quantum defect of the gain medium (2.3). Because of this the absorbed power partially deposits in crystal as a heat:

$$P_{th} = \eta_h P_{abs}, \tag{6.2}$$

where P_{abs} is the absorbed power, η_h is the quantum defect, P_{th} is thermal power.

Under assumption of uniform heat distribution, thermal load can be estimated as follows [Koechner, 1970]:

$$Q_{th} = \frac{P_{th}}{V_{cr}}, \tag{6.3}$$

where V_{cr} is the volume of the active medium.

Since the crystal is pumped with spatially inhomogeneous laser diode array, spatial distribution of absorbed power should also be taken into account. Then, for single-sided pump with Gaussian intensity profile, according to Beer's law we obtain:

$$Q_h(r,z) = -\eta_h \frac{dI_p(r,z)}{dz} = \frac{\eta_h P_p}{\pi \omega_p^2} e^{-2\left(\frac{r}{\omega_p}\right)^2} \sigma_{abs} N e^{-\sigma_{abs} N z}, \tag{6.4}$$

where $I_p(r,z)$ is the pump intensity spatial distribution, z is the direction of propagation of the pump pulse, r is the coordinate in the plane, transversal to the direction of propagation, P_p is the average pump power, ω_p is the pump beam radius at $1/e^2$ level, σ_{abs} is the absorption cross-section of the gain medium, N is the concentration of the active ions, L is the length of the crystal along z-axis.

Since the length of the crystal is small compared to the Rayleigh range of the pump beam, we have assumed in (6.4) ω_p constant along z-axis.

6.2 Results of the simulation

In the model we used following parameters: $\eta_h = \left(1 - \frac{976}{1030}\right) = 0.0524$, $P_p = 200\,\text{W}$, $\omega_p = 1$ mm, $\sigma_{abs} = 1.35 \cdot 10^{-20}\,\text{cm}^2$, $N = 6.87 \cdot 10^{20}\,cm^{-3}$, which corresponds to 2.8% doping, $L = 2\,\text{mm}$. We varied the thickness of undoped slabs in order to evaluate its influence on thermal gradient in the gain medium. The environment is high vacuum, therefore no convection from the faces of the crystal is assumed. Thermal maps are shown in fig. 6.2.

As it can be observed from fig. 6.2, bonded crystals show significantly better heat dissipation compared to convenient crystal. Thermal gradient decreases from 140 K without bonding to 98 K with bonding with 1 mm slabs. Further increase of slab thickness does not improve thermal dissipation and even slightly deteriorates it since thermal gradient is 99 K with 1.5 mm thick undoped slab. This behavior is attributed to the fact that at high thickness copper heat sink, which provides the source of cryogenic cooling is located further from the heat source.

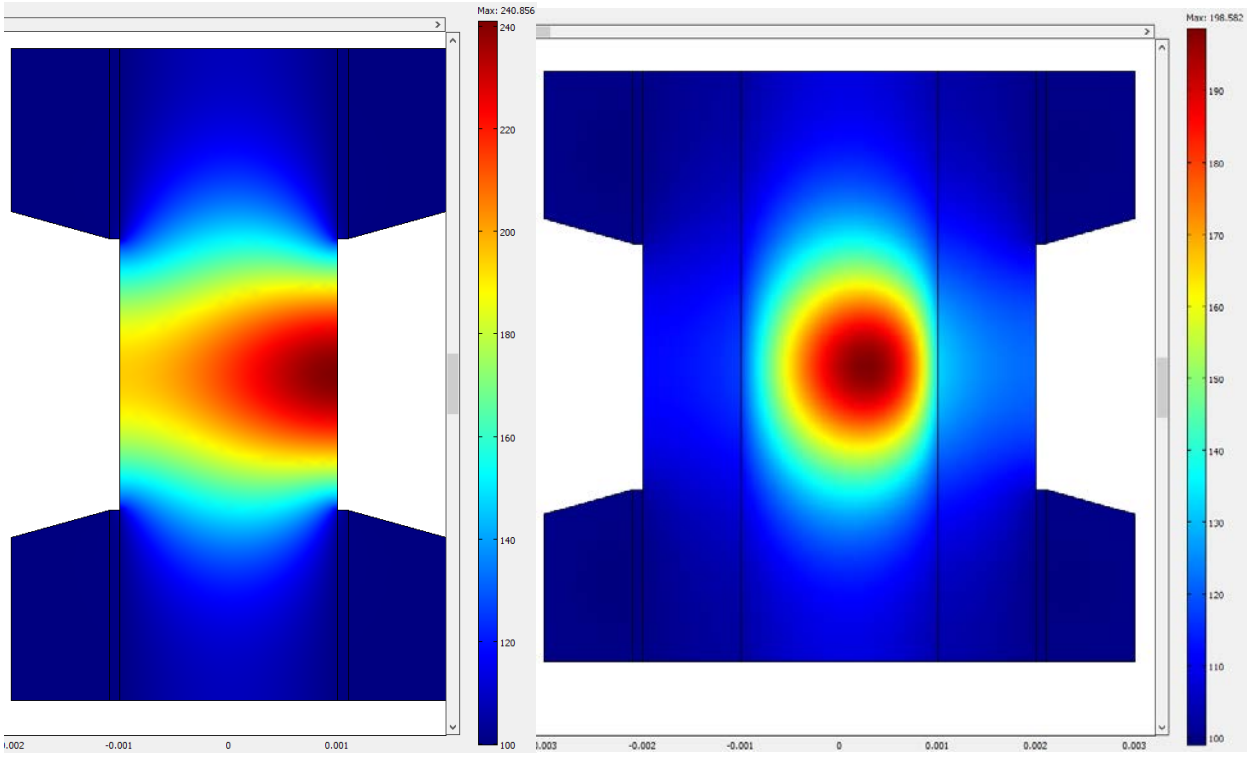

a). 0 mm. $\Delta T = 140K$ b). 1 mm. $\Delta T = 98K$

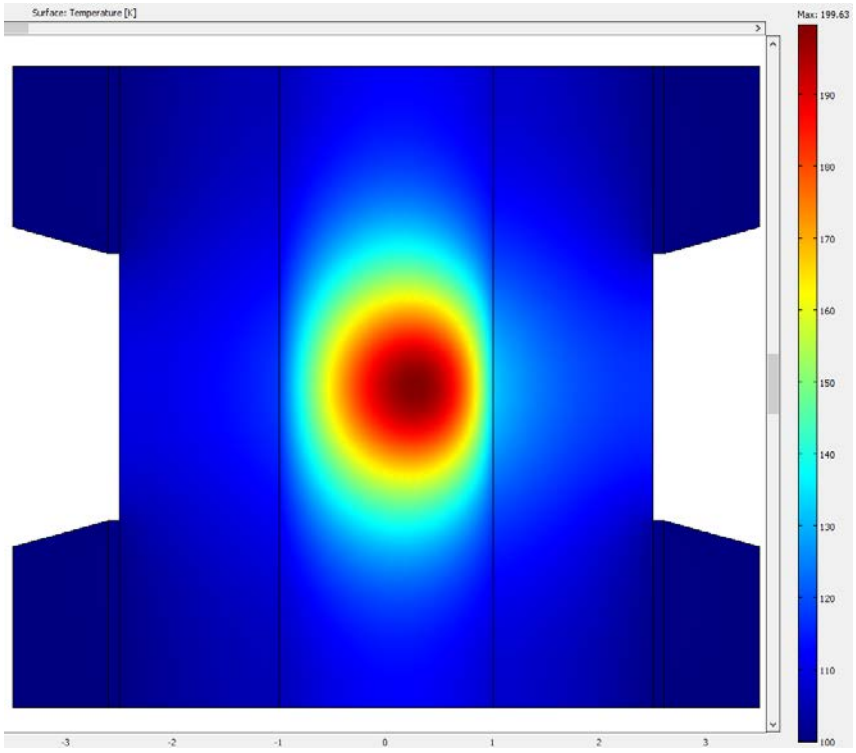

c). 1.5 mm. $\Delta T = 99K$

Fig. 6.2 Thermal maps of laser crystals bonded with blank CaF_2 slabs of different thickness in copper holder under 200 W pump power

Having confirmed positive influence of bonding on thermal behavior of the system, we have fixed the thickness of blank areas to 1 mm and varied the length *L* of the doped region in order to determine the optimal value in terms of heat dissipation. The results of the simulation are presented in fig. 6.3 and indicate gradual scaling of thermal gradient with thickness of active region, which is linked to the fact that thicker gain medium absorbs more pump power. Narrow active region will provide smaller single-pass gain.

In pursuit of smaller thermal gradient in the gain medium we simulated thermal distribution also in case of double-sided pump arrangement, such as has been implemented in RA amplifier [Pugzlys, 2009]. In this case under the same pump power of 200 W heat dissipation must be more efficient since the hottest spots on the crystal are located on both faces of the gain medium. In case of double-sided pump equation (6.4) is modified as follows:

$$Q_h(r,z) = -\eta_h \frac{dI_p(r,z)}{dz} = \frac{\eta_h P_p}{2\pi\omega_p^2} e^{-2\left(\frac{r}{\omega_p}\right)^2} \sigma_{abs} N \left(e^{-\sigma_{abs} N z} + e^{-\sigma_{abs} N (L-z)} \right) \qquad \textbf{(6.5)}$$

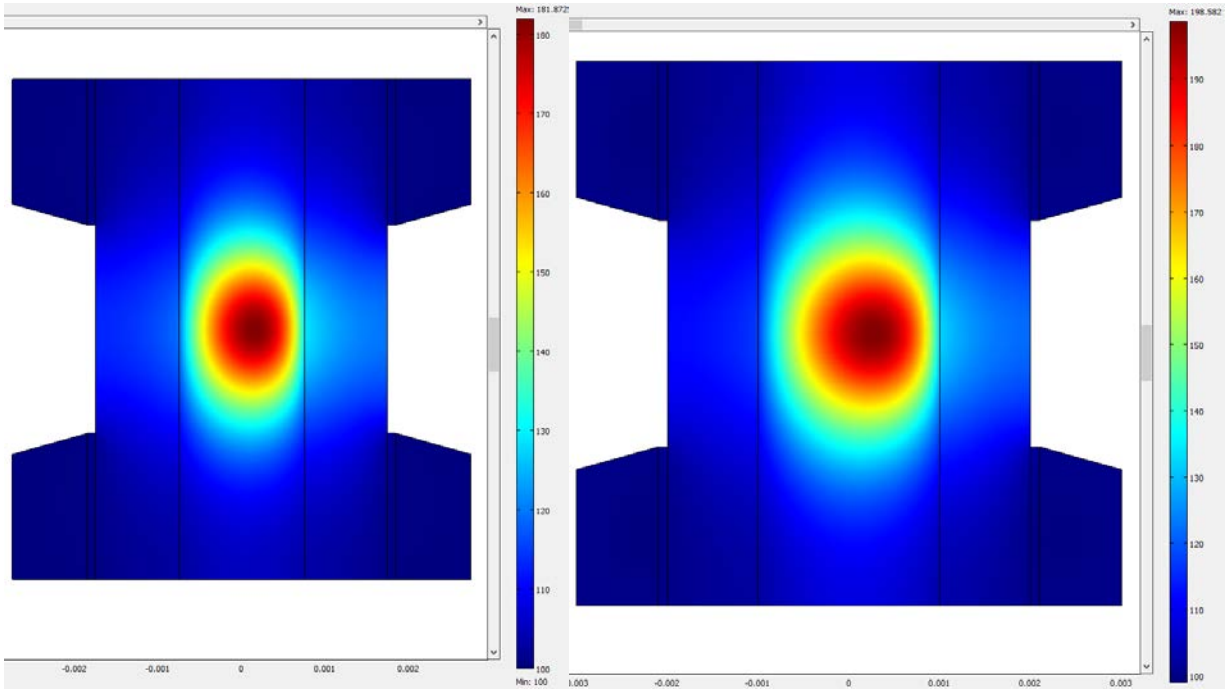

a). 1.5 mm $\Delta T = 82K$ b). 2 mm $\Delta T = 98K$

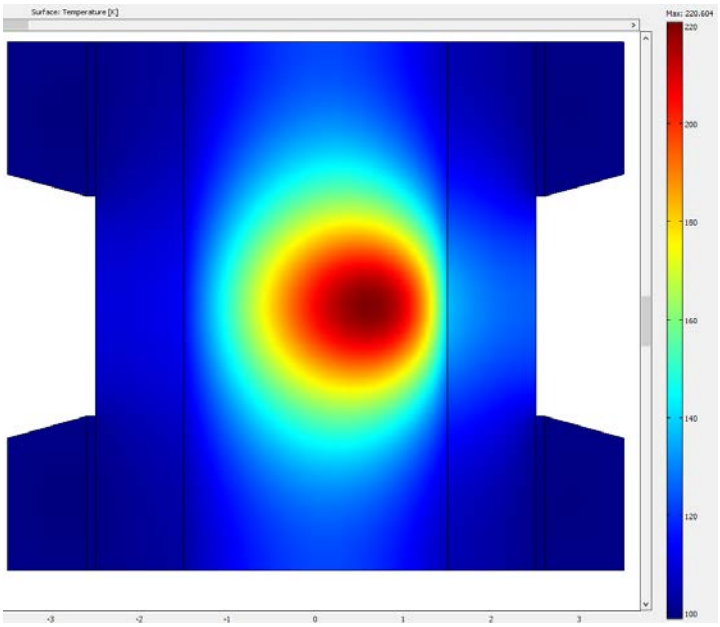

c). 3 mm $\Delta T = 120K$

Fig. 6.3 Thermal maps of laser crystals with different thickness of active region bonded with blank 1 mm thick CaF_2 slabs in copper holder under 200 W pump power

The results for double-sided heat source in comparison to single-sided pump can be seen in fig. 6.4.

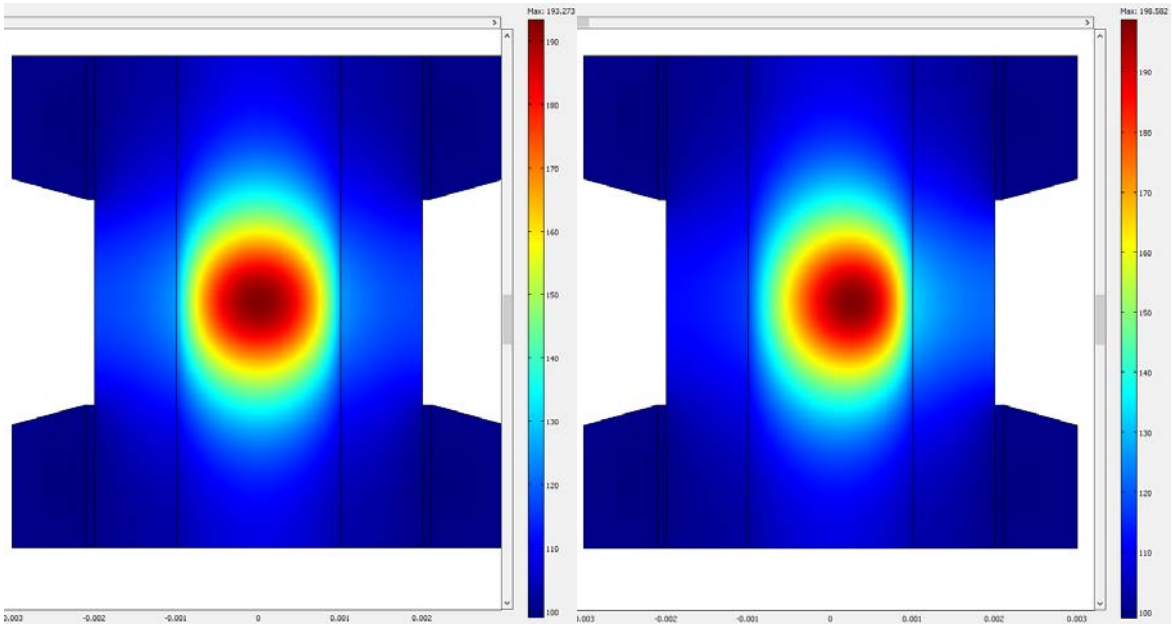

a). Double-sided pump $\Delta T = 93K$ b). Single-sided pump $\Delta T = 98K$

Fig. 6.4 Thermal dissipation in the laser crystal with 2 mm thick active medium bonded with 1 mm thick blank slabs in case of double-sided and single-sided pumping of 200 W

The result of double-sided pumping exhibits lower thermal gradient along with more even heat distribution.

Conclusions

In the framework of the present thesis configuration of multi-pass Yb^{3+}:CaF_2 amplifier with 10 passes has been offered. The bottleneck of low emission and absorption cross-sections has been overcome by employing cryogenic cooling of the active medium.

An issue of spatial gain narrowing was addressed. The alternative multi-pass scheme that allowed expansion of the beam diameter has been offered.

Experimental characterization of the developed system was conducted. Dependence of the small-signal gain of the chosen laser crystal on the LD driving current has been measured. Output cross-section of the beam has been recorded. Dependencies of the output energy on absorbed pump energy and on input pulse energy is measured. Output energy scales with input energy to 100 mJ without substantial saturation, which offers possibility for further increase of output energy.

Developed system delivers 100 mJ output pulses with 500 ps duration at 50 Hz repetition rate, ~10 nm bandwidth centered at 1030 nm.

Output spectrum of 100 mJ pulses was measured and confirmed minor spectral gain narrowing at FWHM level and spectral broadening on the edges of the spectral range, which is attributed to the self-phase modulation effect, which occurs in the beam waist position in the air.

Furthermore, numerical modelling of heat dissipation in laser crystal has been conducted. Thermal performance of the advanced Yb:CaF_2 crystal bonded with undoped CaF_2, which has higher thermal conductivity and serves as a heat sink in lateral direction, was compared to the convenient crystal cooled solely through the contact with copper heat sink. Substantial advantages of thermal bonding of the crystal has been confirmed. Optimal thickness of blank slabs has been investigated and constituted ~1 mm. Thermal distribution in the case of double-sided pumping arrangement was compared with single-sided pump and offered lower thermal gradient in the gain medium than in the latter case.

Outlook

The performance of the developed system can be improved in several ways.

Currently, multi-pass amplifier operates at 50 Hz repetition rate, while our ultimate goal is to reach 100 Hz repetition rate. In order to accomplish this task, we will employ the pump system with emission line at the highest driving currents that matches the zero-phonon line of Yb:CaF_2.

Moreover, undesirable broadening of the output spectrum originates from the SPM effect in the beam waist in the air. In order to eliminate spectral distortions, we will encapsulate the beam path into the vacuum chamber.

Furthermore, we will test the bonded crystals considered in the chapter 6 and compare experimental results with the established theoretical improvements.

Abbreviations

BOYS	Strontium Yttrium Borate
CaF_2	Calcium Fluoride
CPA	Chirped Pulse Amplification
DC	Direct Current
DFG	Difference Frequency Generation
DNA	Deoxyribonucleic Acid
DPSS	Diode Pumped Solid-State
FWHM	Full Width at Half Maximum
GDD	Group Delay Dispersion
GSA	Ground State Absorption
InGaAs	Indium Gallium Arsenide
KLM	Kerr-Lens Mode-Locking
LD	Laser Diode(s)
LN	Lithium Niobate ($LiNbO_3$)
LiSAF	Lithium Strontium Aluminum Fluoride
LiCAF	Lithium Calcium Aluminum Fluoride
LiSGaF	Lithium Strontium Gallium Aluminum Fluoride
MO	Master Oscillator
MP	Multi-Pass
OPA	Optical Parametric Amplification
OR	Optical Rectification
QPM	Quasi Phase Matching
QWP	Quarter-Wave Plate
RA	Regenerative Amplifier
RE	Rare-Earth
RT	Room Temperature
SH	Second Harmonic

SPM	Self-Phase Modulation
SSL	Solid-State Laser
SYS	Strontium Yttrium Silicate
TFP	Thin Film Polarizer
TL	Transform Limited
TM	Transition-Metal
TOD	Third Order Dispersion
YAG	Yttrium Aluminum Garnet
Yb^{3+}	Tri-valent Yb Ion
Yb^{3+}: CaF_2	Yb^{3+}-doped Calcium Fluoride
YLF	Yttrium Lithium Fluoride
ZPL	Zero Phonon Line

Aknowledgements

I would like to express my infinite gratitude to Prof. Andrius Baltuška for opportunity to work in his research group and for sharing his great experience and knowledge. I would also like to thank Dr. Audrius Pugzlys for his comprehensive helpful advising and for priceless help in laboratory.

I am especially grateful to Dr. Giedrius Andriukaitis for patient guidance, daily skillful supervision and friendly atmosphere that is everywhere where he comes.

I also sincerely thank Pavel Malevich, Seyedreza Larimian, Tobias Flöry, Tadas Balciunas, Dr. Skirmantas Ališauskas, Valentina Shumakova for helpful discussions and good friendship that we have established. Special thanks to the whole Ultrafast Laser Group for productive and pleasant atmosphere that prevails at the Institute.

The last, but not the least, my deep respect and gratitude to my parents and my wife for their persistent belief and support.

Reference list

Aggrawal, R. L., *et al*. 2005. “Measurement of thermo-optic properties of Y3Al5O12, Lu3Al5O12, YAIO3, LiYF4, LiLuF4, BaY2F8, KGd(WO4)2, and KY(WO4)2 laser crystals in the 80-300 K temperature range”, *J. Appl. Phys*. 98

Akhmanov, Sergey A. *et al.* 1965. “Observation of parametric amplification in the optical range”, *JETP Lett*., 2, 191

Andriukaitis G. *et al*. 2011. “90 GW peak power few-cycle mid-infrared pulses from an optical parametric amplifier”, *Opt. Lett.* 36, 2755-2757

Balogh, E. *et al.* 2010. Attosecond pulse generation in noble gases in the presence of extreme high intensity THz pulses, *31st European Conf. on Laser Interaction with Matter (XXXI ECLIM)*, Budapest, Hungary, 6–10 Sept. 2010.

Boudeile, J., *et al*., 2008. “Thermal behaviour of ytterbium-doped fluorite crystals under high power pumping”, *Opt. Express* 16, 10098-10109

Brenier, A. and Boulon, G. 2001. “Overview of the best Yb3+-doped laser crystals”, *Journal of Alloys and Compounds* 323, 210-213

Brown, C. David *et al.* 2010. “High sustained average power cw and ultrafast Yb:YAG near-diffraction-limited cryogenic solid-state laser”, *Opt. Exp.*, 18/24

Chaskalovic, J. 2008. *Finite Elements Methods for Engineering Sciences*. Springer Verlag

Chen, X. *et al*. 2010. *Polarization Coupling of Light and Optoelectronics Devices Based on Periodically Poled Lithium Niobate*. ISBN 978-0953-7619-82-4

Chenais, S., *et al*., 2001. “Multiwatt, tunable, diode-pumped CW Yb:GdCOB laser”, *Appl. Phys*. B 72, 389-393

Chenais, S., *et al.* n.d. “On thermal effects in solid state lasers: the case of ytterbium-doped materials”, n.a.

Corning, *CaF_2 Physical and Chemical Properties*, 2003

Davis, R.J. 2001. *Copper and Copper Alloys*, ASM International

Demaria, A.J., *et al*. 1966. Self mode-locking of lasers with saturable absorbers, *Appl. Phys. Lett*. 8, 174-176

Druon, F., *et al*. 2002. “Diode-pumped Yb:Sr3Y(BO3)3 femtosecond laser”, *Opt. Lett.* **27**, 197-199

Druon, F., *et al*., 2009. “Mode-locked operation of a diode-pumped femtosecond Yb:SrF2 laser”, *Opt. Lett*. 34, 2354-2356

Druon, F., *et al*. 2011. “On Yb:CaF2 and Yb:SrF2: review of spectroscopic and thermal properties and their impact on femtosecond and high power laser performance”, *Opt. Mat. Expr*. 1, 489-502

Ebrahimzadeh, M. 2003. *Parametric Light Generation*. Phil. Trans. R. Soc. Lond. A 361, doi: 10.1098/rsta.2003.1284

Fork, R.L. *et al*. 1987. Compression of optical pulses to six femtoseconds by using cubic phase compensation, *Opt. Lett*. 12, 483-485

Fülöp, J.A. *et al.* 2011. Towards generation of mJ-level ultrashort THz pulses by optical rectification, *Opt. Expr.*, vol. 19, #16, 15090

Ghigo, A. *et al*. 2007. “Laser Temporal Pulse Shaping: Comparative Study Between LCM-SLM and DAZZLER Techniques”. *CARE*, Report-2007-032-PHIN

Grilli, R. *et al.* 2009. “Mid-IR ethane detection using a quasi-phase matched LiNbO3 waveguide”, 2009-TD-02

Gulevich, E. *et al.* 1994. “Current state and prospects for tunable titanium–sapphire lasers”, *Proc. SPIE* 2095, 102

Hellwarth, R.W. and McClung F.J. 1962. “Giant Pulsations from Ruby”, *Bull. Am. Phys. Soc.* 6, 414

Hoffmann, M.C. and Fülöp, J.A. 2011. Intense ultrashort pulses: generation and applications, *Appl. Phys.* 44, 083001

Hong, W. *et al*. 2009. Few-cycle attosecond pulses with stabilized-carrier-envelope phase in the presence of a strong terahertz field, *Opt. Express* 17(7), 5139–5146

Honninger, C. *et al*. 1999. “Ultrafast ytterbium-doped bulk lasers and laser amplifiers”, *Appl. Phys.* B 69, 3-17

Ito, M., *et al*., 2004. “Crystal growth, Yb3+ spectroscopy, concentration quenching analysis and potentiality of laser emission in Ca1-xYbxF2+x”, *J. Phys.: Condens. Matter* 16, 1501-1521

Kartashov, D. *et al*. 2012. “Free-space nitrogen gas laser driven by a femtosecond filament”, *Phys. Rev. A*, 86, 033831

Kawanaka, J., *et al*., 2002. “Improved high-field laser characteristics of a diode-pumped Yb:LiYF4 crystal at low temperature”, *Opt. Express* 10, 455-460

Koechner, Walter and Bass, Michael. 2003. *Solid-State Lasers. A Graduate Text*, New-York. Springer-Verlag

Koechner, Walter. 1970. “Absorbed Pump Power, Thermal Profile and Stresses in a cw Pumped Nd:YAG Crystal”, *Appl. Opt.*, 9/6, 1429-1434

Ladison, J. L., *et al*. 2005. "Hardness, elastic modulus, and fracture toughness bulk properties in corning calcium fluoride" in *Proc. SPIE*, Optical Microlithography XVIII(San Jose, CA, USA), pp. 1329-1338.

Lagatsky, A. A., *et al*., “Passive Q switching and self-frequency Raman conversion in a diode-pumped Yb:KGd(WO4)2 laser”, *Opt. Lett*. **25**, 616-618

Lee, Yun-Shik. 2009. *Principles of Terahertz Science and Technology*. Corvallis, Oregon. Springer Science + Business Media, LLC

Lucca, A., *et al*., 2004. “High-power tunable diode-pumped Yb3+:CaF2 laser”, *Opt. Lett*. 29, 1879-1881

Malevich P., *et al.* 2012. “Ultrafast-laser-induced backward stimulated Raman scattering for tracing atmospheric gases”, *Opt. Expr*., 20/17, 18784

Moulton, P.F. 1986. Spectroscopic and laser characteristics of Ti:Al2O3, *JOSA B* 3, 125-133.

Mourou, G. *et al.* 2006. *Chirped Pulse Amplification*. France, ENSTA

National Bureau of Standards, 556 *Thermal Conductivity of Solids*

Nevada Terawatt Facility: http://www.physics.unr.edu/ntf/laser.php

Paschotta, R. 2008. *Encyclopedia of Laser Physics and Technology*. ISBN: 978-3-527-40828-3

Popmintchev, T. *et al*. 2012. “Bright coherent ultrahigh harmonics in the keV X-ray regime from mid-infrared femtosecond lasers”, *Science*, 336, 1287-1291

Popov, P. A., *et al*. 2008. “Thermal conductivity of single crystals of Ca1-xYbxF2+x solid solutions”, *Dokl. Phys*. 53, 198-200

Pugzlys, A. *et al.* 2009. “Spectroscopy and lasing of cryogenically cooled Yb,Na:CaF_2”, *Appl. Phys.*, 97, 339-350

Russbueldt, P., *et al*. 2009. “400W Yb:YAG Innoslab fs-amplifier”, *Opt. Express* 17, 12230-12245

Shank, C.V. and Ippen, E.P. 1974. Subpicosecond kilowatt pulses from a mode-locked cw dye laser, *Appl. Phys. Lett*. 24, 373-375

Siegman, A.E. 1986. *Lasers*, University Science Books, Mill Valley, CA.

Siebold, M. *et al*. 2009. “Yb:CaF2—a new old laser crystal”, *Appl. Phys*. B 97, 327-338

Slack, G. A., 1961. “Thermal Conductivity of CaF2, MnF2, CoF2, and ZnF2 Crystals”, *Phys. Rev.* 122, 1451-1464

Spence, D.E. *et al*. 1991. 60-fsec pulse generation from a self-mode-locked Ti:sapphire laser, *Opt. Lett*. 16, 42-44

Stepanov, A. G. *et al*. 2008. Generation of 30 microJ single-cycle terahertz pulses at 100 Hz repetition rate by optical rectification, *Opt. Lett*. 33(21), 2497–2499.

Stepanov, A.G. *et al*. 2010. Mobile source of high-energy single-cycle terahertz pulses, *Appl. Phys*. B 101(1-2), 11–14

Strickland, D. and Mourou, G. 1985. Compression of amplified chirped optical pulses, *Opt. Commun*. 56, 219-221

Stuart, B.C. *et al.* 1995. “Laser-Induced Damage in Dielectrics with Nanosecond to Subpicosecond Pulses”, *Phys. Rev. Letters*, 74/12, 2248-2251

Treacy, E.B. 1969. “Optical pulse compression with diffraction gratings”, *IEEE J. Quan. Electr.* QE-5, 454-8

Uehara, N., *et al*., 1996. “Spectroscopic measurements of a high-concentration Yb3+:LiYF4 crystal”, *Jpn. J. of Appl. Phys*. Part 2 35, L499-501

Vodopyanov, K.L. 2006. “Optical generation of narrow-band terahertz packets in periodically inverted electro-optic crystals: conversion efficiency and optimal laser pulse format”, *Optics Express* 14 2263–76

Zhang, X.C. and Xu Jingzhou. 2010. *Introduction to THz Wave Photonics*. Springer New York